ADVANCED MATERIALS
www.advmat.de

Materials and Device Engineering Perspective: Recent Advances in Organic Photovoltaics

Ying Zhang, Hao Xia, Jiangsheng Yu, Yang Yang, and Gang Li**

Solar energy is the most promising and ultimate renewable energy resource, and silicon photovoltaic technology has gone through exciting growth globally. Organic photovoltaics (OPVs) provide solar energy solutions for application scenarios different from existing PV technologies. The organic PV technology, with the synergetic progress in the past decades, has now reached 20% power conversion efficiency (PCE), which has the potential to empower serious new applications using the unique features of OPV—light weight, colorful, semitransparent, flexibility, etc. The concise review focuses on recent device engineering progress in OPV technologies. The background of OPV devices and materials, especially recent nonfullerene acceptors, will first be presented; then, in the recent device engineering progress, the focus will be on active layer engineering to control the morphology of OPV, leading to recent 19%–20% efficiency. The parallel progress in bulk heterojunction (BHJ) and sequential layer-by-layer approaches will be summarized. The transparent OPV (TOPV) devices are of great interest with unique features and provide the broadest design space among all solar technologies. This work reviews the TOPV progress covering the active layer and transparent optical structure designs. The future research directions in OPV are discussed with perspective.

1. Introduction

Organic photovoltaics (OPV) are regarded as the competitive next-generation photovoltaics due to their unique advantages, such as semitransparency, flexibility, stretchability, light weight, and low-cost production.[1–6] Since the invention of bulk-heterojunction in 1995, solution-processed OPVs have seen great progress in power conversion efficiencies (PCEs) up to 19–20% through material innovation and device engineering,[7–11] paving toward the future manufacturing. The first layer-by-layer (LBL) OPVs were introduced in 1986 in Tang's landmark work on Applied Physics Letters.[12] The donor/acceptor mixture OPV concept was demonstrated by Hiramoto et al. in 1992 through the co-evaporation of donor and acceptor molecules under high-vacuum conditions.[13] The landmark works of efficient bulk heterojunction (BHJ) polymer solar cells were reported in 1995 by Heeger (polymer:fullerene)[14] and Friend (polymer:polymer).[15] A typical OPV device comprises an electron donor (D) and an electron acceptor (A) material, sandwiched between two electrodes typically with electron and hole carrier transport interlayers. The separated electrons and holes are extracted through external electrodes connected to the device. Historically, significant progress has been achieved across all these components, with particular emphasis on advancements in the light-absorbing layer.

Considering the intrinsic properties of organic materials, these molecules are primarily composed of carbon–carbon double and single bonds arranged along their backbone, and the molecules are held together by Van der Waals forces.[6] Charge transport channels in these materials rely on both inter- and intramolecular interactions.[16] Unlike the free carriers generated in inorganic materials upon light absorption, excitons in organic materials are tightly bound and require a driving force, such as an energy-level offset typically greater than 0.3 eV, to separate. This separation process could often result in significant recombination losses due to the formation of charge transfer (CT) states at D/A interfaces in OPV devices.[17,18] The underlying reason is the lower dielectric constant of organic materials, which remains a key limiting factor in maximizing the photovoltage of OPVs, making them lag behind inorganic solar devices in terms of efficiency. The major breakthrough of the emergence of nonfullerene acceptors (NFAs) is, in part, relieving this driving force concern, which would result in less recombination losses.[19,20] On OPV device progress, the critical role of morphology control in the active layer of OPVs was well recognized since 2005, including molecular orientation, packing, crystallinity, and phase separation.[21] The intrinsically

Y. Zhang, H. Xia, J. Yu, G. Li
Department of Electrical and Electronic Engineering
Research Institute for Smart Energy (RISE)
Photonic Research Institute (PRI)
The Hong Kong Polytechnic University
Hong Kong 999077, China
E-mail: gang.w.li@polyu.edu.hk

Y. Zhang, Y. Yang
Department of Material Science and Engineering
University of California Los Angeles
Los Angeles, CA 90095, USA
E-mail: yangy@g.ucla.edu

The ORCID identification number(s) for the author(s) of this article can be found under https://doi.org/10.1002/adma.202504063

DOI: 10.1002/adma.202504063

short exciton diffusion length of 10–20 nm in organic materials limits the length scale of D and A phase separation, which is largely dictated by thermodynamic molecular interactions. However, a lack of consensus persists regarding the guiding principles of morphology control, stemming from the complex interplay among active-layer components, the miscibility between components and solvents, varying crystallization kinetics, and the challenge of reliably correlating structural properties with device performance. Therefore, advancing OPV efficiency relies on the development of emerging organic semiconductor materials and precise control of the morphology of the OPV active layer, as well as interface engineering—transport layers and device architecture innovations. Despite these challenges, OPVs offer distinct advantages over other photovoltaic technologies, placing them as a promising option for a wide range of applications. One of the most remarkable features of OPV materials is their tunable chemical structure, which allows for adjustable bandgaps. Particularly appealing are low-bandgap materials that extend spectrum absorption into the near-infrared region,[22,23] enabling the capture of more photons and reducing radiative recombination losses. Additionally, the potential for semitransparent OPV (TOPVs) devices opens avenues for applications such as building-integrated photovoltaics (BIPV).[24]

In this review, we highlight recent advancements in the device engineering of OPV technology. We begin the review by examining the development of photovoltaic materials, with particular emphasis on NFAs. Following this, we provide a comprehensive summary of the latest progress in device engineering, focusing on key strategies on mainstream active layer engineering, involving the sequential layer-by-layer approach, multicomponent strategies, and additive and co-solvent methods, all of which have contributed to achieving efficiencies exceeding 20%. Additionally, we review advancements in TOPVs, discussing innovations in active layer design and transparent optical structures. Finally, we offer a future outlook on critical aspects such as materials development, morphology control, and stability within the OPV field.

2. Materials Development

This OPV materials section focuses on the molecular design principles and the evolution of acceptor materials, transitioning from traditional fullerene-based acceptors to advanced NFAs. It highlights key breakthroughs, including 3,9-bis(2-methylene-(3-(1,1-dicyanomethylene)-indanone))-5,5,11,11-tetrakis(4-hexylphenyl)-dithieno[2,3-d:2',3'-d']-s-indaceno[1,2-b:5,6-b']dithiophene (ITIC-families) and Y-series of acceptors. This part also covers the introduction of donor materials, aiming to elucidate their performance optimization mechanisms and outline prospective directions for molecular design.

2.1. Regulation of Bandgap and Energy Level

For ideal active layer materials, the fundamental motivation of molecular design is aimed to achieve complementary absorption spectra between donor and acceptor molecules, maximizing the utilization of solar photons and thereby achieving a high short-circuit current density (J_{SC}) in the device.[25,26] Therefore, bandgap tuning of materials is crucial for optimizing the performance of OPVs. The main methods designed for bandgap modulation typically include frontier orbital hybridization, delocalization of electrons along the conjugated backbone, planarization of molecular structures, and enhancement of quinoid effects. Frontier orbital hybridization theory is a fundamental concept in structural chemistry and plays a crucial role in bandgap modulation for OPV materials. It is widely utilized due to the strong donor–acceptor (D–A) interactions, which can significantly reduce the bandgap, enhancing the material's optoelectronic properties.[27,28] This principle involves chemical bonding between donor units and acceptor units, leading to the highest occupied molecular orbital (HOMO) and lowest unoccupied molecular orbital (LUMO) levels to hybridize. Electrons redistribute to form new HOMO and LUMO levels with a smaller bandgap, the diagram is shown in **Figure 1a**. These new formed energy levels are primarily determined by the HOMO of the donor unit and the LUMO of the acceptor unit.[29] Typically, strong electron-donating units exhibit higher HOMO levels, while strong electron-withdrawing units show lower LUMO levels. Thus, selecting donor and acceptor units with varying strengths enables more room for both bandgap and energy level tuning.[30] Consequently, bandgap modulation and energy level adjustment often coincide (Figure 1b). In an example, Zhu et al.[28] reported an A–D–A type small molecule 3BDDBDT and an A–D–A–D–A type oligomer 5BDDBDT composed of BDT and BDD units (Figure 1c). From 3BDDBDT to 5BDDBDT, the D–A interaction was enhanced, and the HOMO energy level was lifted from −5.37 to −5.27 eV, and the optical bandgap decreased from 2.00 to 1.83 eV, demonstrating effective bandgap modulation. In addition, extending the conjugated backbone can increase the delocalization of π-electrons, allowing the electrons to distribute over a larger area rather than being confined to individual bonds or atoms. As a result, the electron cloud becomes more delocalized along the molecular backbone, leading to a narrower energy level distribution of molecular orbitals. Specifically, this delocalization causes an increase in the HOMO energy level, a decrease in the LUMO energy level, and a consequent reduction in the HOMO–LUMO energy gap.[31,32] Zhou et al. synthesized a series of $(D–A–D)_n$ (n = 1–8) type molecules S1–S8 using thiophene and benzothiadiazole as the basic units.[31] The HOMO energy level of these molecules gradually increases from −5.55 to −4.99 eV and the optical bandgap decreases from 2.46 to 1.69 eV as the conjugated backbone of the molecules is extended. Moreover, strategies aimed at enhancing molecular planarity, such as incorporating rigid structural units or introducing intramolecular noncovalent interactions, are commonly employed to further reduce the bandgap of molecules. The essential reason is that the increase in molecular planarity can strengthen the intermolecular π–π stacking interactions and increase the degree of molecular orbital hybridization.[33,34] To investigate the impact of introducing carbon alkyl chains and oxygen alkyl chains at the 3-position of bithiophene on molecular properties, Guo et al. synthesized the polymers P1, P2, P5a, P5b, and P5c, whose chemical structures are shown in Figure 1c.[34] The results revealed that P1, which possesses two carbon alkyl chains on the bithiophene unit, exhibited the largest optical bandgap of 2.45 eV in its thin film due to significant steric hindrance, resulting in an

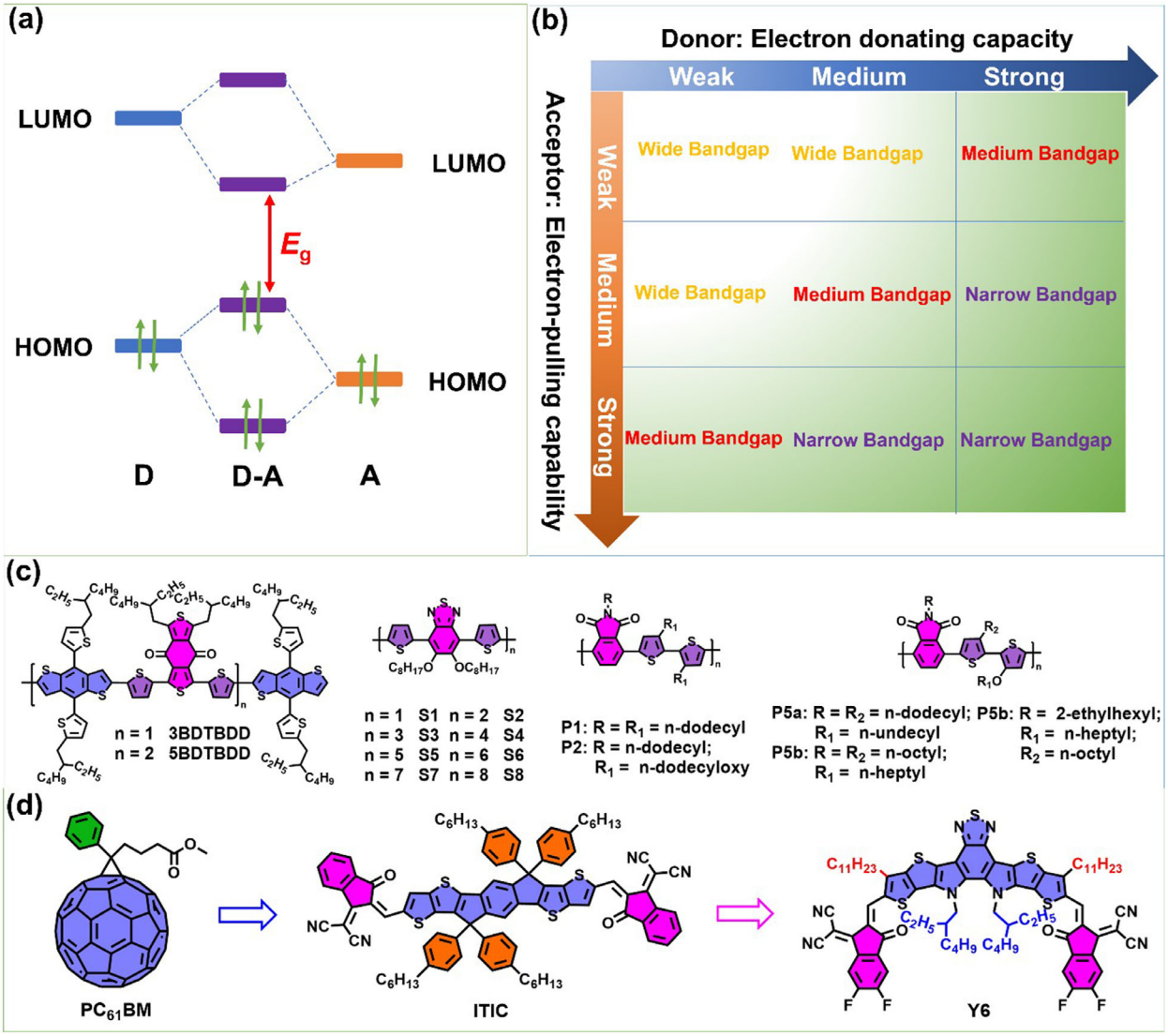

Figure 1. a) Schematic diagram of energy level changes in D–A hybrid orbitals, b) Variation in polymer bandgap with the selection of D and A units. c) The molecular structures of 3BDTBDD, 5BDTBDD, S1–S8, P1, P2, P5a, P5b and P5c. d) The molecular structures of $PC_{61}BM$, ITIC, and Y6.

excessively large dihedral angle of the bithiophene. In contrast, P5a, P5b, and P5c, each featuring one carbon alkyl chain and one oxygen alkyl chain, demonstrated reduced dihedral angles of the bithiophene due to the formation of S···O non-covalent bonds, thereby enhancing the molecular planarity. Consequently, the optical bandgaps of their thin films decreased to 1.85, 1.79, and 1.81 eV, respectively. Furthermore, P2, which incorporates two alkoxy chains, formed two S···O non-covalent bonds, further reducing the dihedral angle of the bithiophene and enhancing the molecular planarity. As a result, the optical bandgap of its thin film was further reduced to 1.65 eV. Moreover, people demonstrated that the incorporation of units with quinoid structural features enhances quinoid resonance, destabilizing the aromatic ground electronic state, strengthening the intramolecular charge-transfer (ICT) effect, and effectively reducing the material's bandgap. This approach is widely utilized in OPV to design donor–acceptor materials with narrower bandgaps.[35,36] For instance, on the basis of the IDIC structure, Liu et al. introduced two thieno[3,4-b]thiophene units with strong quinoidal characteristics, synthesizing the small-molecule acceptor ATT-2.[36] The thin-film absorption of ATT-2 spans from 300 to 940 nm, and its optical bandgap is reduced to 1.32 eV, compared to 1.62 eV for IDIC. When blended with PTB7-Th as the donor material, the opaque device achieved a PCE of 9.58%, accompanied by a notable J_{SC} of 20.75 mA cm^{-2}.

2.2. Molecular Structure Tuning the Crystallinity of Active Layer Materials

Controlling the crystallinity of active layer materials in OPVs is crucial for optimizing charge transport, exciton diffusion, and thus in turn affects the device performances.[37,38] Researchers have demonstrated that introducing rigid and planar

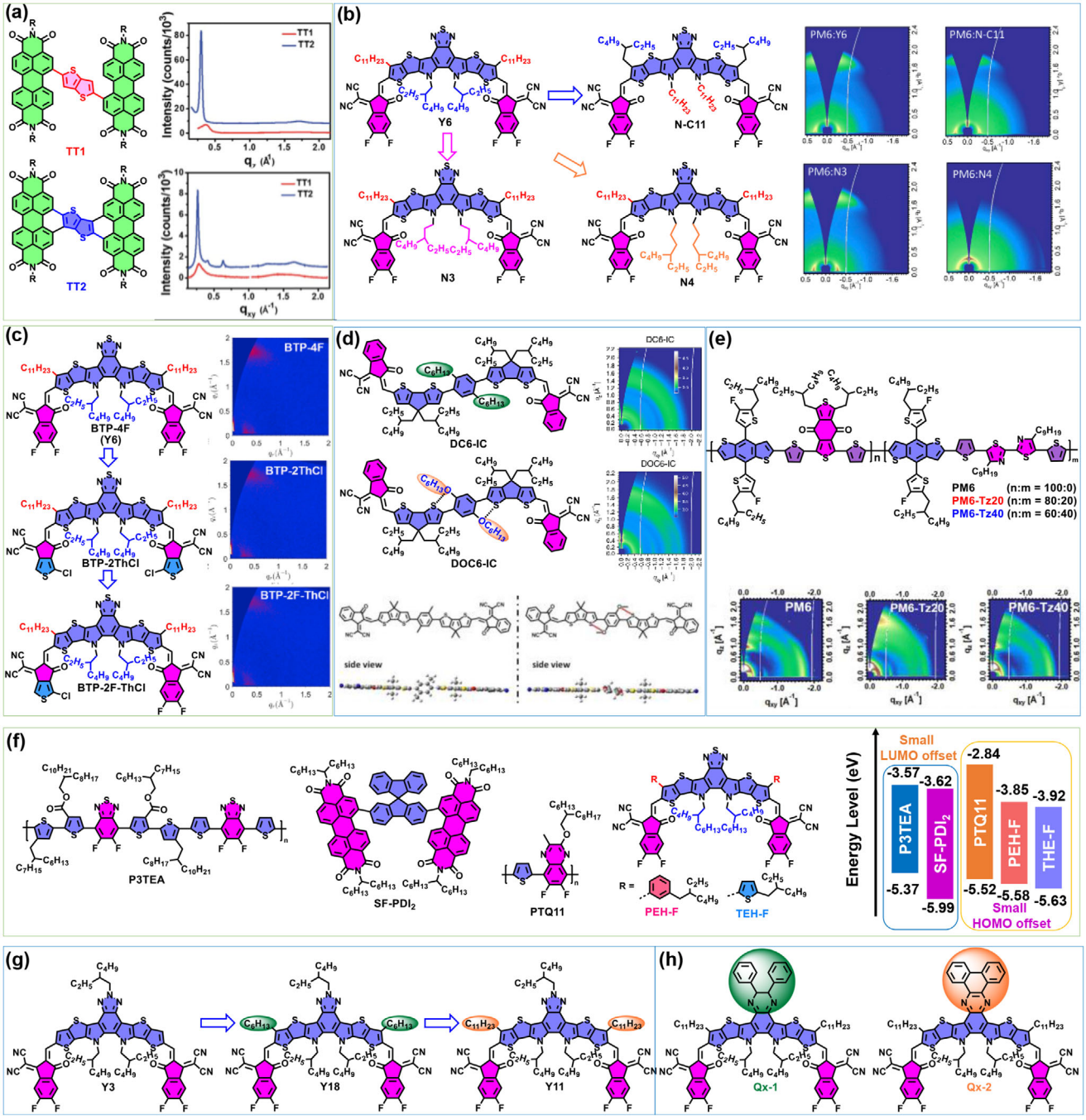

Figure 2. Strategies for modulating crystallinity and energy levels through molecular design. a–e) Approaches for tuning crystallinity, including molecular engineering, side-chain modification, and conformational control. Reproduced with permission.[39] Copyright 2016, Royal Society of Chemistry, Reproduced with permission.[42] Copyright 2019, Cell Press, Reproduced with permission.[45] Copyright 2022, Wiley-VCH, Reproduced with permission.[48] Copyright 2019, Springer Nature, and Reproduced with permission.[51] Copyright 2020, Wiley-VCH. f–i) Representative molecular structures designed for precise energy level regulation.

π-conjugated backbones can enhance π–π stacking, promoting higher crystallinity. Incorporating a π-bridge can reduce excessive crystallinity, ensuring balanced charge transport and mechanical flexibility.[39–41] For example, Hartnett et al. synthesized TT1, which connects two PDI units via a bithiophene linker, and TT2, where two PDI units are fused with a bithiophene moiety, as shown in **Figure 2**a.[39] GIWAXS measurements revealed that, compared to TT1, TT2 exhibited significantly enhanced (100) diffraction peak intensity and more pronounced (010) diffraction peaks, indicating stronger π–π stacking interactions between the large planar TT2 molecules. Moreover, adjusting the length and branching of side chains impacts solubility and crystallinity.[42–44] Shorter chains or linear chains generally increase crystallinity, while branched chains can disrupt excessive

packing and improve film uniformity. Jiang et al. reported N-C11, N3, and N4, investigating the relationship between linear chains, branched chains, and the branching position with solubility and crystallinity, as shown in Figure 2b.[42] The results showed that, compared to linear chains, branched chains significantly improved solubility while reducing crystallinity. Furthermore, increasing the branching position distance improves the solubility of the molecule. Additionally, end-group engineering serves as a key strategy for tuning molecular crystallinity. Substituting terminal groups in small molecules with electron-withdrawing or electron-donating units modifies molecular packing behavior, thereby influencing crystallinity.[45–47] For instance, Lu et al. reported three small molecular acceptors, named BTP-4F, BTP-2ThCl, and BTP-2FThCl, by modifying the end groups from IC-2F to CPTCN-Cl, as shown in Figure 2c.[45] The crystallinity of BTP-2ThCl and BTP-2FThCl with CPTCN-Cl end group is weaker than that of BTP-4F. In addition, incorporating non-covalent interactions (such as S···O, S···N, and F···H) into the main chains not only enables fine-tuning of molecular energy levels and bandgaps but also significantly enhances the planarity of the molecular backbone, thereby improving molecular crystallinity.[48–50] Huang et al. synthesized DC6-IC without noncovalent bonding and DOC6-IC with noncovalent bonding (S···O), as shown in Figure 2d. The S···O bonding reduces the torsion angle between the DTC unit and the benzene ring, which improves the planarity of the molecular skeleton of DOC6-IC and, consequently, its crystallinity.[48] Notably, in the molecular design of polymers, incorporating different copolymer units with alternating crystalline and amorphous segments can strike a balance between order and disorder. This approach facilitates optimizing both structural organization and flexibility.[51–53] Guo et al. developed a novel terpolymer donor PM6-Tz20 by a simple terpolymerization method, as shown in Figure 2e.[51] They found that the introduction of an appropriate amount of DTBTz units could effectively modulate the molecule's crystallinity, molecular orientation, and aggregation behavior.

2.3. Strategies for Reducing Energy Loss through Molecular Design

Energy loss (E_{loss}) in OPVs sets a fundamental limit on the maximum achievable PCE. Compared to higher efficiency counterparts like silicon, GaAs, and perovskite solar cells, OPVs typically experience larger E_{loss} due to more pronounced non-radiative recombination and less efficient charge generation and separation processes.[19,54–58] Minimizing E_{loss} through molecular design and reducing non-radiative decay pathways is essential for improving the V_{OC}, enhancing energy utilization, and narrowing the efficiency gap between OPVs and other photovoltaic technologies. Studies indicate that V_{OC} is positively correlated with the energy level difference between the HOMO of the donor and the LUMO of the acceptor. A decreased energy offset (ΔE_{LUMO} or ΔE_{HOMO}) will reduce the energy loss while ensuring that the excitons can be separated efficiently.[54] Hence, designing donor and acceptor molecules with reduced HOMO and LUMO offset to minimize the driving force required for charge separation can reduce energy loss. Liu et al. reported a highly efficient OPV based on a novel polymer named P3TEA and an SMA named SF-PDI2 and an SMA named SF-PDI2, as shown in Figure 2f. Despite the ΔE_{LUMO} between the two materials is only 0.05 eV, fast and efficient charge separation can still be achieved. As a result, the non-fullerene OPV device demonstrated a low energy loss of 0.61 eV (with a bandgap of 1.72 eV and a V_{OC} of 1.11 V).[19] Sun et al. designed and synthesized two A–DA'D–A type SMAs with different conjugated side chains, namely, PEH-F and TEH-F, as shown in Figure 2f. The PEH-F with benzene ring side chains exhibits smaller ΔE_{HOMO} (0.06 eV) when paired with PTQ11. Despite this small ΔE_{HOMO}, efficient exciton dissociation and hole transfer are successfully realized, resulting in a reduced energy loss of 0.511 eV for PTQ11:PEH-F-based OPVs. Moreover, in OPVs, energetic disorder arises from structural heterogeneity, variations in molecular packing, or thermal fluctuations, leading to dispersive energy levels in donor and acceptor materials. A large energetic disorder broadens the distribution of these energy levels and reduces the sharpness of energy level alignment. This necessitates a larger energy offset for efficient charge separation, which directly diminishes the V_{OC}.[55] Y3, Y11, and Y18 were synthesized to investigate the impact of alkyl chains at the terminal positions of the central core on device performance (Figure 2g).[56] In Y3, the absence of terminal alkyl chains increased rotational freedom of the core and end groups, causing structural disorder and a low V_{OC} of 0.81 V in PM6:Y3 devices. Conversely, Y11 and Y18, with terminal alkyl chains, exhibited restricted rotation, reduced energetic disorder, improved charge carrier mobility, and a higher V_{OC} of 0.84 V. Furthermore, reorganization energy (λ) in solar cells represents the energy required to adjust molecular geometries during charge transfer, which is closely related to charge separation efficiency.[57] A high λ indicates significant structural changes, resulting in inefficient charge separation and increased energy losses. Additionally, a high λ increases the probability of non-radiative recombination by offering pathways for energy dissipation as heat. In contrast, a lower λ reduces the energy barrier for charge transfer, improving exciton dissociation and charge carrier generation efficiency. Shi et al. provided a good example with the synthesis of two acceptors, Qx-1 and Qx-2, featuring a larger volume and a more rigid Qx central core, as shown in Figure 2h.[58] By suppressing molecular vibrations, particularly the stretching of C—C bonds, both acceptors demonstrated significantly lower reorganization energies during photoelectric conversion compared to the conventional Y6 acceptor. As a result, the PM6:Qx-2 system achieved an impressive PCE of 18.2% with a low energy loss of 0.482 eV. Additionally, suppressing electron–phonon coupling is essential for minimizing energy loss. Electron–phonon coupling describes the energy-dissipating interactions between electrons and atomic vibrations in materials. Strong coupling promotes charge scattering, heat dissipation, and non-radiative decay, ultimately reducing energy efficiency. For this example, Jiang et al. systematically developed SMAs AQx-2, AQx-6, and AQx-8[59] with varying alkyl side-chain lengths to investigate the correlation between side-chain length, electron–phonon coupling strength, and device energy losses. Their study demonstrated that an appropriate extension of the alkyl side-chain can simultaneously reduce free volume ratio while restricting molecular motion, thereby weakening electron–phonon coupling without compromising nanomorphology. As a result, the D18:AQx-6-based device achieved an outstanding PCE of 18.6% with a remarkably low energy loss of 0.518 eV, benefiting from

both reduced free volume and favorable morphology enabled by precise alkyl chain engineering.

2.4. Transition from Fullerene Acceptors to NFAs

Fullerene derivatives (e.g., $PC_{61}BM$, as shown in Figure 1c) were the dominant acceptor materials in the early stages of OPV development due to their advantages, including excellent electron transport properties and high electron affinity.[60,61] However, fullerene-based acceptors face several limitations. First, their absorption spectrum is narrow, primarily confined to the UV–visible region, resulting in poor utilization of near-infrared light. Second, they exhibit difficulty in energy level tuning, posing challenges in achieving ideal energy level alignment with donor materials, which contributes to high energy losses. Moreover, they suffer from poor morphological stability due to a tendency for self-aggregation, which adversely impacts the long-term stability of the devices.[62,63] When paired with typical donor materials such as P3HT and PTB7-Th, fullerene-based acceptors typically achieved efficiencies below 10%.[64,65] These limitations prompted researchers to explore NFAs. From 2015, NFAs such as ITIC and Y6 (as shown in Figure 1c) have emerged as a transformative force in the field of OPV, offering significant advantages over traditional fullerene-based acceptors, e.g., tunable energy levels, broad absorption spectra, and excellent morphological stability.[66,67] Advances in molecular engineering, such as end-group modification, backbone tuning, and side-chain optimization, have further improved the photophysical properties, charge transport, blend morphology, and energy loss of NFAs.

In 2015, Lin et al. pioneered the synthesis of ITIC, an A–D–A structured molecule based on an indacenodithieno[3,2-b]thiophene (IDTT) core, marking the dawn of the high-efficiency NFA era.[68] ITIC addressed several limitations of traditional fullerene acceptors, such as weak absorption in the visible and near-infrared (NIR) regions, limited tunability of electronic properties, and morphological instability. ITIC exhibits several key characteristics that make it a highly effective NFA. Central to its performance is the IDTT core, which possesses strong electron-donating capabilities, paired with electron-withdrawing dicyanoindanone end groups, creating a pronounced push–pull (D–A) effect. This structural design, combined with the steric hindrance introduced by the four alkyl chains attached to the sp^3-hybridized carbons on the IDTT core, prevents H-aggregation and promotes J-aggregation. As a result, the absorption spectrum is redshifted, enabling ITIC to achieve broad absorption spanning 600–800 nm. This significantly enhances light-harvesting efficiency and maximizes photocurrent generation. In addition, the energy levels of ITIC can be finely tuned through core and end-group engineering. This tunability allows for optimal alignment with the HOMO and LUMO levels of donor materials, reducing energy losses during charge transfer and improving the V_{OC} of the device. Furthermore, ITIC demonstrates high electron mobility, a critical factor for efficient charge transport and extraction. The extended conjugated system of the IDTT core facilitates electron delocalization and efficient transport, while the dicyanoindanone end groups lower the LUMO level, enhancing electron affinity. The symmetric molecular structure further promotes ordered face-on molecular stacking in the solid state, which not only boosts electron mobility but also minimizes charge recombination. This ordered crystalline structure enhances the FF, contributing to higher overall device efficiency. The introduction of ITIC propelled OPV efficiencies beyond 12%, a significant milestone at the time.[2] Its success inspired extensive research into the A–D–A framework, including modifications to the central unit's ring size, alkyl side chains, and end groups.[69]

In late 2010s, Y-series NFAs were reported, further introducing an innovative A–DA′D–A structure with a lower optical bandgap, significantly broadening the absorption spectrum. Its planar backbone and 3D multi-modal aggregation enabled high electron mobility, while reduced energy loss ensured high V_{OC}.[20,70] Since then, the Y family has expanded through modifications to end groups, side chains, and conjugated backbones, producing derivatives with record-breaking PCEs exceeding 20%. Notable representatives include Y7,[71] BTP-eC9,[72] and L8-BO,[73] which exemplify the potential of this groundbreaking class of materials. The success of Y6 has not only established new benchmarks for OPVs but has also significantly advanced our understanding of the molecular design principles governing NFAs performance. The key features that establish Y6 as a milestone material are as follows: 1) Ultra-broad and strong absorption. Y6 exhibits an exceptionally broad absorption spectrum, extending into the 800–1000 nm range, which is significantly red-shifted compared to ITIC. This is attributed to the much stronger D-A push-pull effect within the Y6 molecule, similar to ITIC, but with a larger fused-ring core that enhances electron delocalization. Additionally, the incorporation of a benzothiadiazole unit with pronounced quinoidal effects further extends the absorption range. The extinction coefficient of Y6 is also significantly improved, increasing from 1.5×10^5 cm^{-1} for ITIC to 2.5×10^5 cm^{-1} for Y6.[74,75] This improved light-harvesting capability directly contributes to an increased J_{SC}. 2) Molecular packing and high charge mobility. Y6 features a highly rigid conjugated backbone, which promotes ordered molecular arrangement in the solid state, thereby enhancing crystallinity. The large fused-ring units in Y6 exhibit high planarity, facilitating tight molecular packing through π–π interactions and reducing disordered regions. Moreover, the introduction of appropriate alkyl side chains on thiophene and pyrrole not only ensures good solubility but also optimizes molecular packing through steric effects, further improving crystallinity. Unlike ITIC, which often exhibits amorphous behavior due to the significant steric hindrance caused by its four alkyl chains attached to two sp^3-hybridized carbons, Y6 demonstrates strong face-on molecular packing. This ordered arrangement facilitates efficient charge transport, enhancing its performance in organic solar cells. Furthermore, researchers have demonstrated that Y6-based molecules adopt versatile packing configurations, including end-to-end, core-to-end, and core-to-core interactions, which give rise to a well-defined 3D ordered network structure.[76–78] This packing diversity could provide more intermolecular charge transport pathways, thus in turn benefits charge transport. 3) Low energy loss. Y6 exhibits low energy loss due to its well-aligned energy levels with donor materials, e.g., PM6, PTQ10, D18, including cases where $\Delta E_{HOMO} \approx 0$. This alignment minimizes energy loss during exciton separation and suppresses charge recombination. Furthermore, the alkyl chains on its thiophene units enhance conformational

stability, reducing energy disorder and leading to a sharper EQE tail.[77] Furthermore, Y6 exhibits a significantly higher photoluminescence quantum yield (PLQY) of ≈5%, which is substantially greater than that of the ITIC series (e.g., the PLQYs for ITIC, IEICO-4F, and IT-4F are 1.4%, 0.4%, and 1.4%, respectively).[79] A higher PLQY indicates a larger external quantum efficiency of electroluminescence (EQE_{EL}), which correlates with lower non-radiative energy losses in the device. 4) High morphological stability under thermal and/or light. The rigid conjugated backbone of Y6 enhances thermal stability and minimizes structural deformation under light or heat. Its high molecular symmetry further prevents degradation and isomerization in the solid state. Tight molecular packing improves mechanical and morphological stability, and the unique 3D network structure resists phase separation under thermal or photonic stress.[80]

2.5. Overview of Donor Materials

Three donor categories dominate the field: conjugated polymers, small molecules, and oligomers. Conjugated polymers exhibit excellent film-forming properties and tunable optical absorption, whereas small molecules are recognized for their well-defined structures, high purity, and crystalline properties. Additionally, oligomers—specialized molecules with multiple repeating units, well-defined structures, and relatively high molecular weights—have attracted significant attention.

2.5.1. Conjugated Polymers

The D–A strategy is a widely used approach for designing conjugated polymers. By alternating electron-rich units and electron-deficient units in the polymer backbone, a strong ICT effect is achieved, resulting in narrow bandgaps and enhanced light absorption. In recent years, with the extensive development of narrow-bandgap non-fullerene acceptors, there has been a growing demand for wide-bandgap polymer donors to achieve broader absorption spectra. Polymers based on weak electron-withdrawing units, such as 1,3-bis(thiophen-2-yl)-5,7-bis(2-ethylhexyl)benzo [1,2-c:4,5-c′]dithiophene-4,8-dione (BDD), quinoxaline (Qx), and dithieno [3′,2′:3,4;2′′,3′′:5,6]benzo[1,2-c][1,2,5]thiadiazole (DTBT), including PM6, PTQ10, PBQx-TF, D18, and their derivatives, have been extensively studied. In 2012, Qian et al. first introduced the polymer donor PBDB-T, which was based on BDT and BDD units (**Figure 3a**).[81] Subsequently, researchers extensively modified the side chains of BDT, leading to the development of high-performance polymer donors such as PM6[82] and PM7.[83] In 2020, Liu et al. reported a novel donor polymer, D18, based on DTBT and fluorinated BDT units (Figure 3a).[84] Binary device using D18:Y6 achieved a remarkable PCE of 18.22%. In 2018, Sun et al. developed a new low-cost polymer donor, PTQ10, based on quinoxaline and thiophene units (Figure 3a).[85] PTQ10 was synthesized through a two-step reaction with a high overall yield, showcasing significant potential for commercial production. In addition, new wide-bandgap polymer systems like L1-S[86] and PNTB6-Cl[87] have also been introduced, with binary OPVs achieving PCEs exceeding 17%. These polymers, with their wide bandgap absorption characteristics, effectively complement narrow-bandgap Y6-series acceptors, resulting in a broader absorption spectrum and enhanced J_{SC}. Moreover, their solution-state absorption spectra typically show temperature dependence, indicating strong pre-aggregation behavior. This characteristic facilitates the formation of optimal blend morphology with high phase purity in the active layer, thereby enhancing device performance.

2.5.2. Small Molecule Donors

Small-molecule donors have attracted much attention because of their well-defined structures and reproducible synthesis. However, most of the current high-performance small molecule donors are based on the BDT series, adopting the A–π–D–π–A configuration. The BDT unit serves as the central D core, cyanide ester, or rhodanine derivatives, etc., as the electron-withdrawing end group (A), and oligothiophene as the π-bridge. Among these, the BDT unit serves as the core building block, making its modification a key focus of research. Common strategies include halogenation, alkyl chain modulation, and asymmetric substitution. Additionally, significant attention has been given to optimizing electron-withdrawing end groups. These modifications have been shown to modulate the energy levels and crystallinity of the molecules, thereby enhancing their photoelectric properties. Lu et al. synthesized two small-molecule donors, BTR and BTR-Cl (Figure 3b),[88,89] Chlorination of the BTR molecule led to a significant decrease in its energy levels, while simultaneously improving its crystallinity and aggregation orientation. Consequently, the PCE of the BTR-Cl-based device was 13.61%, while that of the BTR-based device was only 10.61%. Li et al. synthesized TB and TB-F with asymmetric structures.[90] It was found that the asymmetric structures were able to modulate the interaction between donor and acceptor molecules, resulting in a uniform vertical phase distribution. A champion efficiency of 17.0% was achieved for the TB-F:L8-BO-based OPVs. In addition, porphyrin-based molecules such as ZnP-TBO[91] have demonstrated superior photovoltaic performance due to their excellent light-absorbing properties, making them ideal donor materials for constructing highly efficient all-small-molecule OPVs.

2.5.3. Oligomer Donors

Research on oligomers has gained significant attention in recent years due to their potential to bridge the gap between small molecules and polymers in OPVs. These materials combine the precise molecular structure of small molecules with the excellent film-forming ability of polymers. However, oligomeric donor materials have been relatively underexplored, with high-performance donors mainly consisting of oligomeric thiophenes, oligomeric BDTs, and D–A block oligomers. For example, Kan et al. synthesized the donor DRCN5T using oligomeric thiophenes as the molecular backbone. When blended with $PC_{71}BM$, the resulting OPVs achieved a PCE of 10.08%.[92] Yang et al. synthesized the donor DRTB-T using an oligomerized BDT unit as the molecular backbone.[93] DRTB-T exhibited a wide bandgap of 2.0 eV, and devices based on its blend with IDIC achieved a PCE of 9.08%. Subsequently, derivatives such as DRTB-T-C4, DRTB-T-C6, and DRTB-T-C8 were developed to investigate the

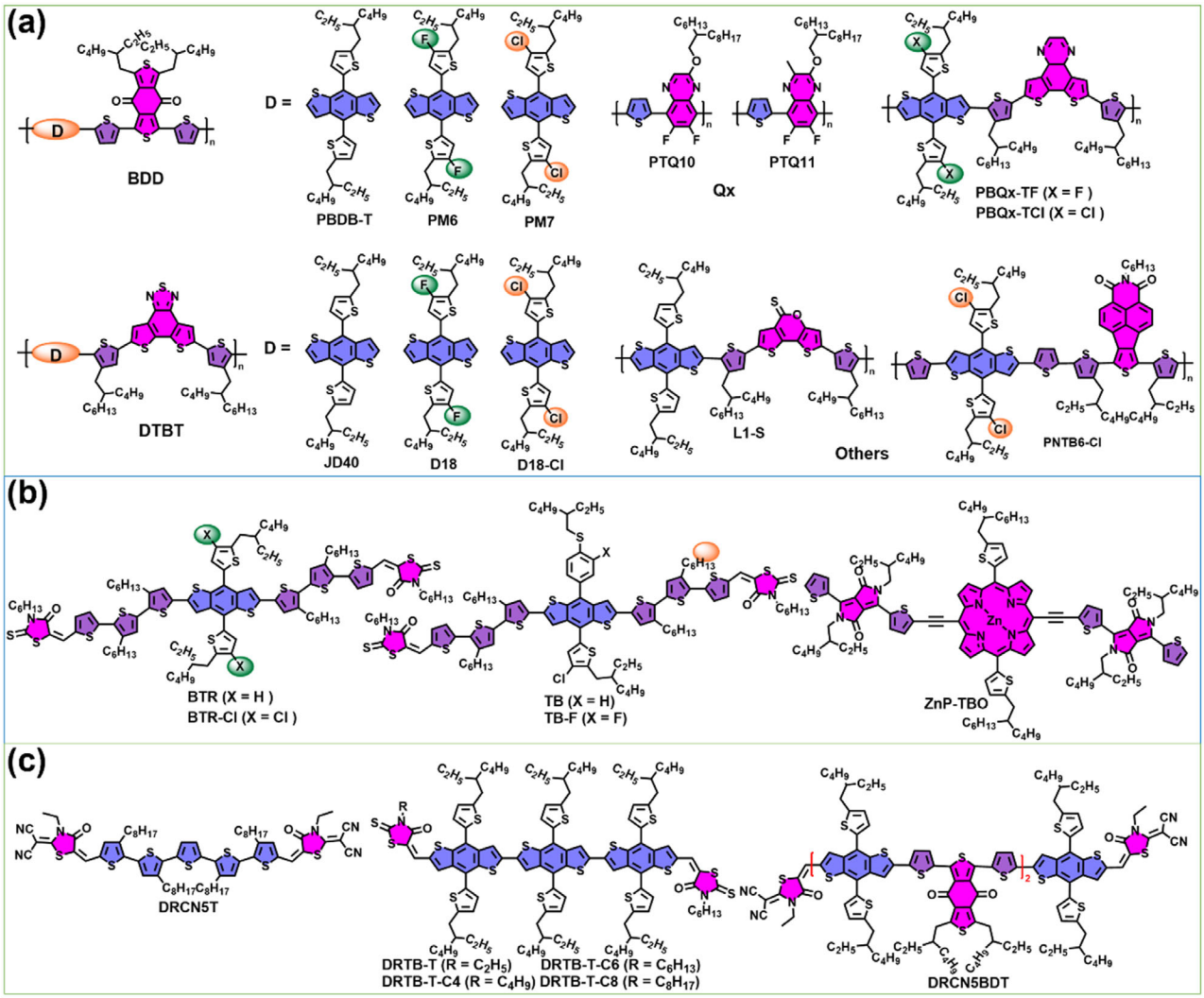

Figure 3. Representative high-performance a) polymer donor materials; b) small molecular donor materials and c) oligomer donor materials.

effect of alkyl chains on the electron-withdrawing end groups on the molecule's aggregation behavior.[94] In addition, Xia et al. reported an A1-D-A-D-A-D-A1-type block oligomer, DRCN5BDT, constructed with BDT and BDD as D and A units and cyanorhodanine as the terminal group. By blending DRCN5BDT with Y6 and optimizing the active layer morphology, a binary device efficiency of 14.04% was achieved.[95]

3. OPV Morphology Control

Morphology control is a critical factor in optimizing the performance of OPVs. The nanoscale phase separation between the donor and acceptor materials directly impacts charge generation, transport, and recombination processes. Achieving an ideal morphology involves balancing domain size, purity, and continuity to maximize PCE. In the very beginning era of fullerene-based OPV systems, people realized that morphology manipulation, including crystallinity, molecular packing, and phase separation, has been demonstrated to contribute to many PCE milestones in the OPV field. Numerous strategies have been proposed to enhance the crystalline and manipulate the phase separation behavior to enhance the photovoltaic performance, including adjusting the host solvents, tuning the ratio of donor-to-acceptor, adjusting the solvent additive, introducing a third component, and various post-treatment methods. Summarization of recent progress of device engineering with major emphasis on morphology control is crucial to further pave the way towards OPV commercialization. In this section, we will explore key strategies for fine-tuning morphology, including sequential deposition, multicomponent optimization, and additive engineering. The most significant progress of each approach will be outlined and discussed.

3.1. Planar OPV Device

Although solution-processed OPV has been dominated by the BHJ structure for decades, in recent years, the planar morphological structure approach has been rebirthed and has become a hot research topic. The possibilities offered by the

sequential deposition have provided impressive results in terms of both efficiency and stability. Parallel to the BHJ structure, planar structure using sequential layer-by-layer (LBL) processing has attracted increasing attention due to its great potential to achieve an ideal phase separation with more pure domains, which would be favorable to charge transport. Unlike the conventional one-step blend deposition (BHJ), the LBL approach involves depositing the donor and acceptor materials in separate layers, enabling greater control over phase separation and interfacial properties. Up to now, the efficiencies via the LBL process can achieve over 19%–20% PCE, gaining growing interest in the OPV field.[96,97] This planar OPV concept was first realized by C.W. Tang in 1979 (published in 1986) through vacuum evaporation of donor and acceptor molecules, which achieved a PCE of ≈1%.[12] Limited interfacial area between the donor and the acceptor in bilayers results in reduced exciton splitting relative to that in BHJs. This planar structure gives a very sharp D:A interface and thus limits the D/A interfaces for charge separation. In 2009, Ayzner et al. made the very early attempt to demonstrate that all-solution processed sequential cell depositing fullerene ($PC_{61}BM$) atop polymer (P3HT) without disrupting the underlying layer could achieve comparable efficiencies (3.5%) relative to the BHJ device.[98] This solution-processed bilayer study enables the formation of a p–i–n vertical phase separation, providing greater flexibility in controlling quasi-solid-state interdiffusion between donor and acceptor materials through the use of orthogonal solvents, thermal annealing, and optimization of individual active layer thicknesses. This challenges the conventional focus on BHJs as the optimal architecture for polymer-fullerene solar cells. In this example, Ayzner et al emphasized the role of thermal annealing as a driving force to promote the fullerene crystallinity and intermixing into the bottom layer of polymer scaffold, thus forming so called quasi-bilayer geometry.[99] This work provides an initial insight into the different morphology formation mechanisms, with the two processing routes (BHJ and bilayer) constructing nanoscale networks in fundamentally different ways, thereby offering a comparative perspective on the traditional BHJ approach. In 2015, the same group further advanced their approach by proposing the use of a mixed solvent for the upper fullerene layer, enabling more precise control over the interdiffusion between donor and acceptor materials.[100] A secondary solvent, 1-butanol, which exhibits good solubility for the underlying polymer, is selected to dilute the primary solvent, 2-chlorophenol. The latter has excellent solubility for fullerene but low solubility for polymers. The synergetic effects facilitate controlled swelling of the underlying polymer layer. As a result, this well-established sequential deposition design successfully achieved an impressive device PCE of 6%. Lee et al. went beyond conventional upper-layer tuning by employing an immiscible solvent strategy to create a nanoporous architecture within the P3HT layer.[101] This approach enabled fullerene molecules to infiltrate the voids within the polymer network, significantly enhancing the donor–acceptor interfacial area. With these bilayer design principles in mind, the PCEs of PSCs processed through bilayer methods have since improved rapidly. For example, Zhan et al. advanced the PCE of OPVs to 8.6% using PTB7-Th as donor and $PC_{71}BM$ as acceptor.[102]

With the advent of NFAs, strategies previously employed in fullerene-based systems can be adapted and expanded. Additionally, the versatile molecular design of NFAs introduces greater flexibility in tailoring solubility properties, opening up new possibilities for meeting the requirements of orthogonal solvent systems. For example, Cui et al. designed and synthesized the conjugated polymer PBDB-TFS1, which exhibits low solubility in most common solvents and dissolves only in heated o-dichlorobenzene (o-DCB). In contrast, IT-4F, used as the upper acceptor, is highly soluble in various organic solvents such as tetrahydrofuran (THF).[103] This donor–acceptor systems in bilayer OPVs enables the use of orthogonal solvents: a mixed solvent of THF with a small amount of o-DCB or chlorobenzene (CB) for the upper and lower layers, respectively. IT was found that THF evaporates rapidly, while *o*-DCB facilitates the penetration of IT-4F molecules into PBDB-TFS1 regions. X-ray photoelectron spectroscopy (XPS) measurements reveal that the enriched acceptor layer is predominantly located near the cathode side (as illustrated in **Figure 4a**), enhancing charge transport and extraction. This favorable phase separation results in a significantly improved PCE of 13.0%. Later on, people find that orthogonal solvent screening plays a less critical role in LBL-processed devices. In this scenario, Fu et al. achieved high-performance LBL OPVs by utilizing PM6 as the donor and Y6-BO as the acceptor, both processed with chlorobenzene (CF). This approach yielded an impressive PCE of 17.2%, surpassing that of their BHJ counterparts.[104] These findings underscore the critical role of the solvent additive e.g., 1,8-diiodooctane (DIO) with higher boiling point in the interdiffusion process during the casting of the top Y6-BO layer. DIO, with its superior solubility for Y6-BO, facilitates the downward penetration of more Y6 molecules due to its extended evaporation time, promoting the formation of sufficient intermixing areas to enhance charge separation.[105] Researchers have also utilized solid additives in the upper to facilitate the molecular competitive self-organization process of small molecules, thereby regulating crystallinity and vertical phase separation.[106] Tuning the miscibility among components proves to be crucial in the LBL process. Zhan et al. demonstrated that interactions between acceptor molecules significantly influence the phase separation within the LBL active layer.[107] To achieve a higher concentration of acceptors at the top, they designed a second acceptor, BTP-S2, which exhibits stronger molecular interactions with the host acceptor BO-4Cl than with the host polymer PM6. BTP-S2 was incorporated with BO-4Cl as the top layer. The strong interactions among the acceptor molecules help retain a greater acceptor content at the top during the swelling-induced diffusion of the second layer, as evidenced by time-of-flight secondary ion mass spectrometry (TOF-SIMS) in Figure 4b. This process promotes a favorable vertical p–i–n phase separation, thereby endowing the LBL devices with excellent charge transport and extraction properties. As a result, an impressive PCE of 18.16% was achieved in the LBL device. Excitingly, LBL method has shown tremendous potential for the fabrication of upscaled OPVs.[108] This advantage arises from the independent processing of the two layers, with the first layer undergoing straightforward solution evaporation-induced crystallization. Furthermore, this approach minimizes complex material interactions and mitigates the excessive phase separation issues often encountered in BHJ coating. Benefiting from the suitable vertical phase separation achieved through the LBL method, Min's group demonstrated excellent compatibility between the LBL approach

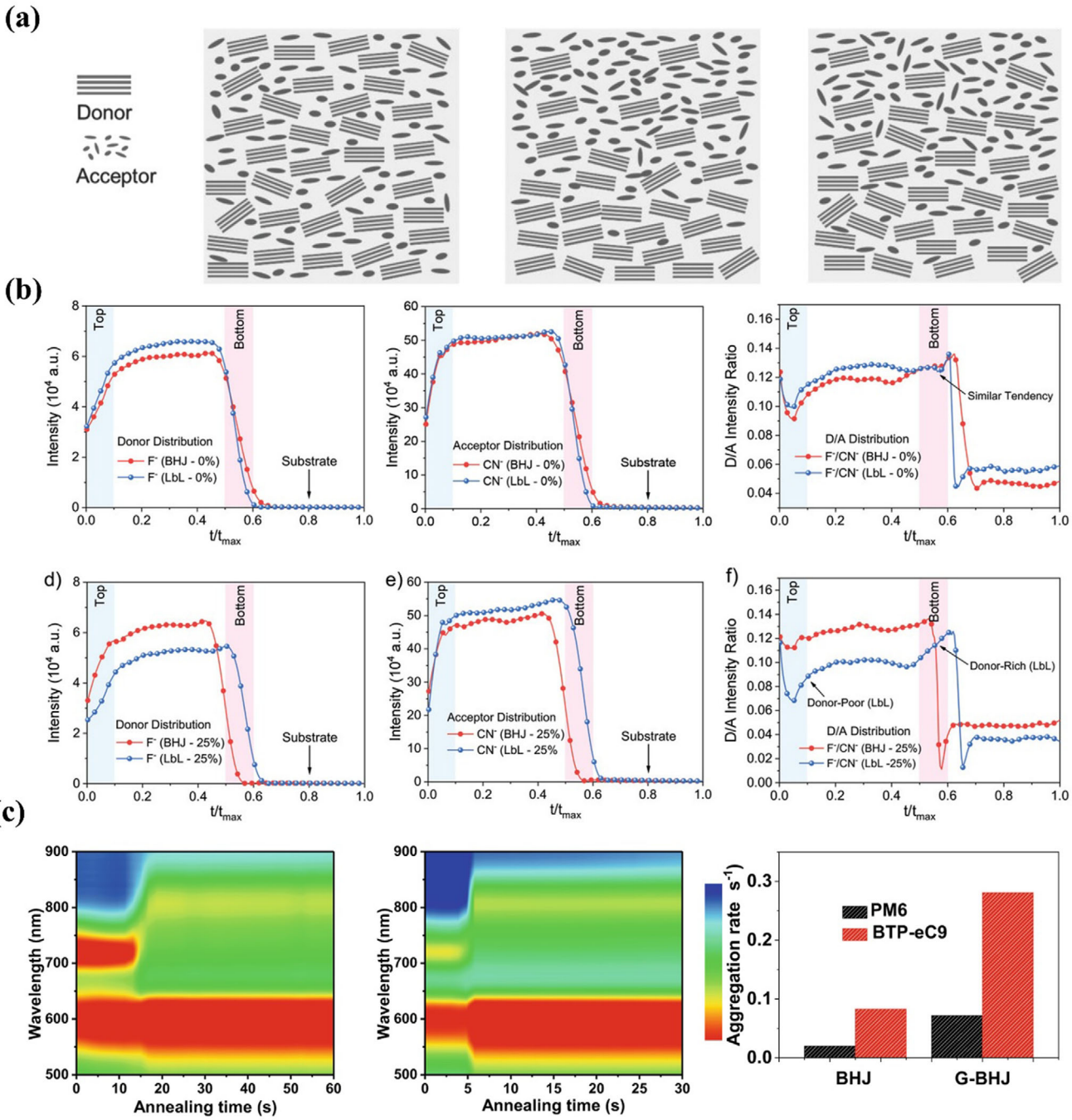

Figure 4. a) Schematic diagrams of film morphology in BHJ and LBL film without *o*-DCB, and with 5% *o*-DCB, respectively, based on PBDB-TFS1/IT-4F. Reproduced with permission.[103] Copyright 2018, Wiley-VCH. b) TOF-SIMS ion yield of F^- and CN^- as a function of sputtering time for BHJ and LBL films. Reproduced with permission.[107] Copyright 2021, Wiley-VCH. (c) Time-resolved UV-vis absorption spectra of optimized BHJ, G-BHJ OPVs films and aggregation rate of PM6 and BTP-eC9 in optimized BHJ and G-BHJ active layers. Reproduced under the terms of the CC-BY Creative Commons Attribution 4.0 International license.[110] Copyright 2021, Springer Nature.

and the blade coating technique. This strategy resulted in a remarkably high PCE of 11.86% for a large-area module device with an active area of 11.52 cm^2, based on PM6/Y6 OPVs, effectively addressing the challenge of PCE retention when transitioning from small-area devices to their large-area counterparts.[109] Zhang et al. provided in-depth insights into the morphological evolution of LBL constituents during the open-air blade coating process, tracking the transition from solution to solid state using in situ UV–vis absorption measurements.[110] Their study revealed that achieving balanced crystallization kinetics between the donor and acceptor layers is crucial for forming an optimal vertically graded phase separation, which is demonstrated

in Figure 4c. With a focus on tuning film formation kinetics, Li's group tailored the drying dynamics of the upper acceptor layer by combining the polymeric molecule PY-IT and the small molecule BTP-eC9. The larger PY-IT molecules tend to self-aggregate first due to their limited downward diffusion, subsequently serving as seeding sites for the crystallization of BTP-eC9. This approach facilitates the formation of an ideal p–i–n structure, with more n-type regions located near the cathode and more p-type areas closer to the anode. To deepen the understanding of the working mechanisms from a physics perspective, Jen and colleagues employed ultrafast transient absorption spectroscopy to investigate charge dynamics in planar–mixed heterojunction (PMHJ) structures realized via the LBL method.[111] Their findings revealed that recombination loss pathways, particularly those related to the relaxation from charge transfer states to triplet states, are effectively suppressed in the PMHJ architecture due to reduced D/A mixed interfaces compared to BHJ counterparts. This suppression minimizes energy loss, leading to enhanced V_{OC}. As a result, OPVs featuring a PMHJ active layer composed of the polymer donor D18 and T9TBO-F/Y6-O alloys achieved exceptional PCEs exceeding 19%. This provides a clear explanation of how a limited D/A interface can still achieve significant gains in both photocurrent and photovoltage. Thus, the LBL design rules open up an entire new avenue of morphology control in processing OPV active layers.

3.2. Multicomponent Strategy

In the beginning, the primary limitation of the PCE in OPV devices lies in the intrinsically narrow spectral absorption range of organic materials compared to that of inorganic semiconductors, such as silicon or perovskites. To address this, an additional component with complementary absorption has been proposed for incorporation into the binary system to extend the solar spectrum absorption range. Koppe et al. were the first to report the use of a near-infrared (NIR) low-bandgap polymer, PCPDTBT, incorporated into the binary blend P3HT:$PC_{61}BM$ to form a ternary system. This approach enhanced NIR absorption and consequently increased the J_{SC} of the ternary device.[112] This increase in J_{SC} is not only attributed to the complementary absorption of the donor molecules but also benefits from charge transfer between guest and host, which leads to decreased charge recombination. Later on, people found addition of third components can control OPV nanomorphology, e.g., molecular crystallinity, molecular packing, and phase separation, which could govern the charge-transfer and/or energy-transfer mechanisms. In principle, however, it is acknowledged that the understanding of nanomorphology control in binary systems remains incomplete, and the addition of a third component further complicates morphology control due to the intricate thermodynamic interactions among materials in BHJ blends. Aiming to investigate the operation mechanisms of the ternary strategy in a simplified way, people propose three main morphological models as follows: cascade model, alloy model, and parallel-like model based on the spatial arrangement of the components.[113] Since the cascade model describes the interfacial area between the D and A without significant morphological effects, we will focus on the alloy and parallel-like models, which were primarily realized during the fullerene era. In 2011, Khlyabich et al. discovered that the V_{OC} values in polymer-fullerene OPVs could be tuned by varying the relative content of different fullerenes in a single system.[114] Subsequently, the same group demonstrated that the composition-dependent V_{OC} originated from the tunable LUMO and HOMO energy levels of the mixed composites, where two fullerene derivatives, ICBA and $PC_{61}BM$, formed an organic alloyed phase. In contrast to the alloy model, researchers observed a different mechanism in ternary OPVs.[115] Here, the V_{OC} of ternary OPVs is typically pinned to the two subcells, while the J_{SC} is nearly equivalent to the sum of the subcell contributions. To explain this phenomenon, the concept of a parallel-like BHJ model was introduced, proposing a scenario in which the two subcells operate independently.

However, a significant challenge arises in this context: identifying the factors that influence potential morphology models during the material selection process, especially when screening is based on established OPV materials. Addressing this issue is crucial for advancing the design and optimization of high-performance multicomponent OPVs. In 2015, researchers discovered that compatibility plays a pivotal role in alleviating morphology perturbations in polymer multi-donor and fullerene-based OPV systems.[116] They proposed that compatible polymer donors with the same BDT unit in structure, characterized by favorable molecular orientation and crystallite size, can help preserve the pre-existing favorable morphology. When these introduced donors exhibit complementary absorption and well-aligned energy levels with the host materials, they facilitate efficient charge transfer and enhanced photocurrent generation without creating morphologically induced disorder. These findings are consistent with Thompson's 2014 study, which emphasized that the compatibility between two polymers is essential in determining the final alloyed morphology, in particular, where similar surface energies were identified as a key factor in enhancing molecular compatibility.[117] These examples suggest that similar surface energies and structural similarities—such as core molecular structure and orientation—serve as straightforward indicators of good compatibility and are empirical hallmarks of the alloyed model in ternary OPVs. However, However, an exception exists where similar molecular structures are not the determining factor for alloy formation. Liu et al. first introduced a ternary blend of two NFAs with different core backbones—SdiPBI-Se and ITIC-Th—along with the polymer donor PDBT-T1. This combination achieved a high PCE of 10.1% in the ternary device.[118] Morphology characterizations demonstrate that these two acceptors are well mixed into one homogenous phase, and V_{OC} can be tuned almost linearly to the weight ratio of mixed acceptors. Therefore, for NFA-ternary OPVs, recent discoveries have provided new insights into conventional models. At the same time, the mechanistic understanding of NFA-ternary OPVs has been revisited and refined, as NFAs differ significantly from fullerenes in many critical properties, such as optical characteristics, packing modes, and electrical behavior.

People put more effort into the thermodynamic interaction, e.g., miscibility between organic materials that could play a key role in driving phase separation.[119] For instance, materials with good miscibility tend to produce smaller, less defined phase domains in a BHJ thin film. In contrast, immiscible materials

typically result in larger phases with greater purity. In a typical system consisting of two polymers and one small molecule, the two polymers tend to initially form separate scaffolds due to their long, entangled chains, which limit their interpenetration. As a result, a parallel arrangement could be one possible model. Therefore, our focus here is on the alloyed model consisting of one polymer donor and two molecules. For example, Hou and coworkers reported the combination of two miscible NFAs IEICO and IT-M, which both have the same central unit.[120] The suppressed crystallinity of IT-M can be observed by transmission electron microscope (TEM) after adding IEICO because a homogenous acceptor phase is formed. In another example, the miscible guest component could balance domain size and crystallinity of the OPV blend. Liu et al. introduced two structurally miscible NFAs. The host material, MeIC, is highly crystalline, which tends to promote strong phase separation.[121] In contrast, the guest material, ITCPTC, exhibits weak crystallinity, allowing it to intermix with MeIC. This intermixing helps to control excessive domain growth while preserving charge transport pathways. As a result, an impressive FF of 78.2% was achieved. One should note that the charge transport pathways can be occasionally destroyed if the intermixing is not well controlled, e.g., too mixing of polymer donor and acceptor would lead to poor carrier transport and, thus, device FF. Thus, creating independent crystalline domains for efficient charge transport pathways is crucial. In one approach, this problem was circumvented by introducing a less miscible acceptor with donor in P3HT:IDTBR:IDFBR ternary blend, where differential scanning calorimetry measurements (DSC) showed IDFBR is more miscible with P3HT and was able to diffuse into the crystalline P3HT domains (**Figure 5a**), while IDTBR is highly self-aggregated.[122] At higher compositions of IDFBR, the IDTBR can be driven into crystalline domains separated outside P3HT domains, forming P3HT:IDFBR mixed domains for charge separation and relatively pure IDTBR with a higher LUMO level for efficient charge transport. This concept was further demonstrated by Zhu's group.[123] BTR exhibited good material mixing with NITI, resulting in finer phase separation, which is typically considered unfavorable for charge transport. In contrast, $PC_{71}BM$, with its higher surface energy, displayed isotropic and superior transport properties and more readily phase-separated from the donor. As confirmed by bright-field and high-angle annular dark-field (HAADF) TEM images (Figure 4b), a nanomorphology emerged where $PC_{71}BM$ aggregates were present and phase-separated from the donor, creating efficient carrier transport pathways. The role of $PC_{71}BM$ as a morphology mediator has been demonstrated in many ternary OPVs containing NFA binary mixture.[124]

So far, one is widely adopted that the use of two miscible NFAs-induced homogenous phases has become a universal guideline for well-working ternary OPVs, which have gained popularity and high efficiency. The universal validity and feasibility of these miscibility-guided morphology manipulation is confirmed repeatedly with analogous findings, particularly in one polymer and two NFAs systems. After entering Y6-containing OPVs that typically exhibit strong aggregation, researchers made many attempts to get deeper insights into the working mechanisms from a thermodynamic perspective. These efforts include investigating differences in crystallization dynamics among components to fine-tune crystallinity and phase separation probing from solution to solid state during spin coating process or blade coating. For instance, Chen et al. synthesized a novel molecule, BTO, to be incorporated into the PM6 and Y6 binary blend. BTO shares the same end groups and a similar core unit with Y6 but features greater coplanarity.[125] In situ UV–vis absorption characterization revealed that BTO could extend the crystalline growth window from solution to solid state in the PM6:Y6:BTO blend and enhance its overall crystalline (Figure 5c), which is attributed to the strong intermolecular interactions between BTO. Similarly, crystallization-induced phase separation was demonstrated by Liu and coworkers. They introduced a more crystalline polymer donor, D18, with poor solubility into the PM6:L8-BO system.[126] D18, a polymer known for its strong temperature-dependent aggregation behavior, is expected to crystallize first as the solvent evaporates. These unperturbed donor fibrils act as seeding sites, facilitating the arrangement of both the polymer and acceptors, thereby further enhancing crystallization. As a result, photo-induced force microscopy (PiFM) revealed a dual-fibril morphology with reduced mixing domains (Figure 5d). These finer, crystalline fibril pathways enable efficient charge transport and suppress charge recombination, leading to an outstanding fill factor (FF) of 81.9%. Jiang et al. advanced the PCE of ternary OPV towards 20% via using symmetric and asymmetric NFAs mixing via constructing a fibrillar nanostructure.[127] Fu et al. also demonstrated that two well-miscible isomeric NFAs, BTP-eC9, and o-BTP-eC9, contribute to complementary crystallinity and favorable fibril nanostructure, enabling high FF and V_{OC} through the strategic selection of a third component.[128] The advantageous fibril nanostructure in Y-series OPVs can be more easily predicted due to the fact that Y6 and its analogs often adopt polymer-like motifs, as evidenced by the analysis of their corresponding single-crystal structures.[129] Fibril nanostructure tuning in Y-series OPVs appears to serve as a key guideline for understanding bicontinuous structures, ultimately leading to high efficiencies. These possibilities demonstrate that morphology optimization can simultaneously maximize the three key device parameters—V_{OC}, FF, and J_{SC}—or improve some of them in OPVs. This is achieved while ensuring the optical properties (e.g., absorption) and energetic properties (e.g., energy levels) of the components remain fundamentally valid. Notably, although the mixing of two donors or acceptors in a ternary blend is often detrimental, it can occasionally be beneficial when these materials exhibit good miscibility. Generally, such miscible systems containing two NFAs have enabled impressive efficiencies in OPVs approaching 19–20%.[130,131]

3.3. Additive and Solvent Engineering

Back in 2005, researchers found that solvent solvent-annealed vapor-assisted strategy could induce the assembly of polymer scaffold and increase the crystallinity of the active layer, first boosting PCE over 4.4%, which was the highest at that time.[21] This discovery can potentially enable people to shed light on morphology tuning. Inspired by this strategy, in 2007, solvent additives, e.g., alkane dithiols with high boiling points, were demonstrated to modulate the crystallinity of the organic component, increasing device PCE from 2.8% to 5.5% in the PCPDTBT:$PC_{71}BM$ OPV system. Since then, the addition of solvent additives has

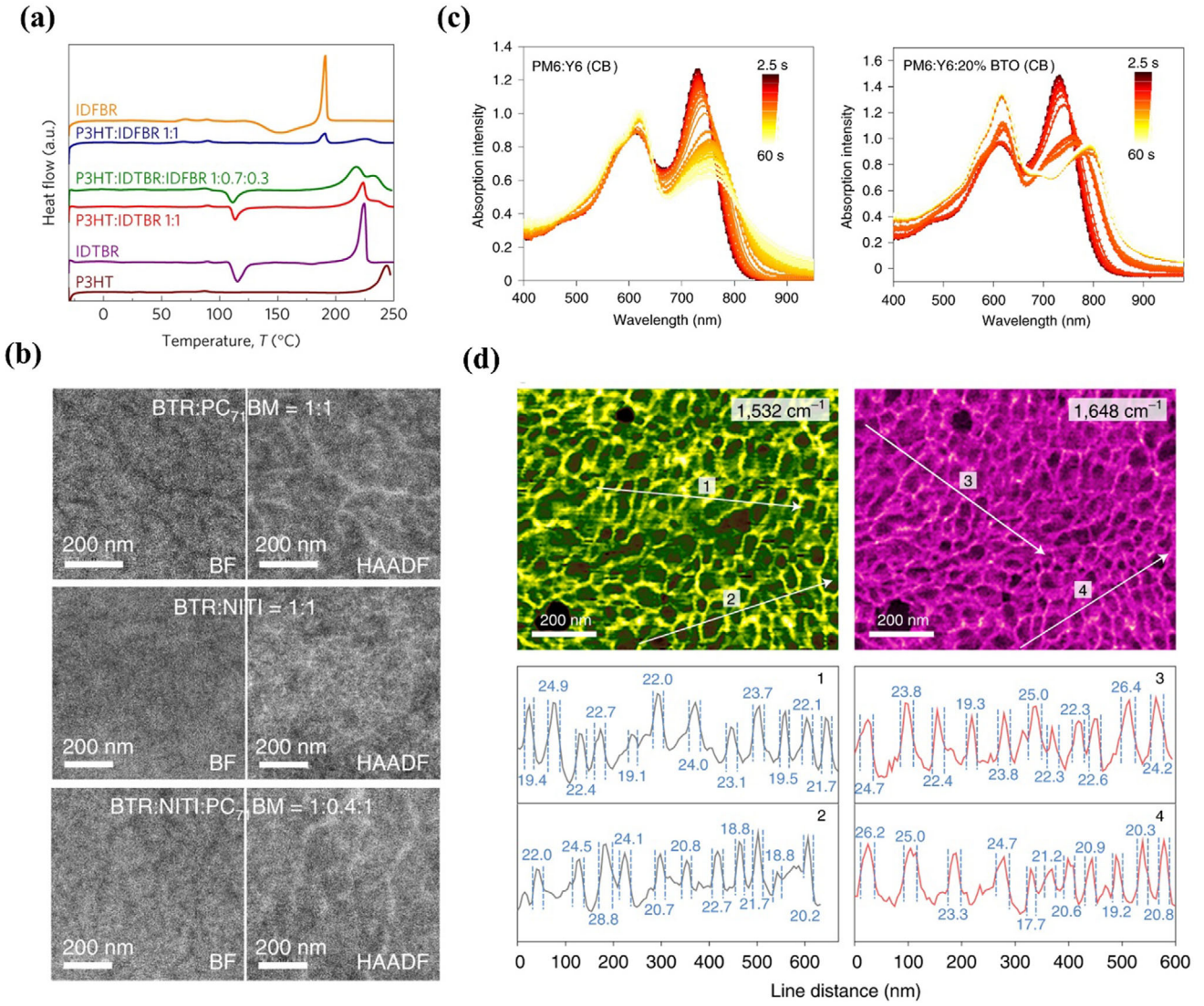

Figure 5. a) The first DSC heating profiles of individual P3HT, IDTBR, and IDFBR, along with binary P3HT:IDTBR, P3HT:IDFBR and ternary P3HT:IDTBR:IDFBR blends. Reproduced with permission.[122] Copyright 2016, Springer Nature. b) Bright-field (BF, left column) and HAADF (right column) TEM of the binary and ternary blends. Reproduced with permission.[123] Copyright 2018, Springer Nature. c) In situ UV–visible absorption of PM6:Y6 and PM6:Y6:20% BTO evolution from the solution (2.5 s) to the film (60 s). The color scale bar represents time. Reproduced with permission.[125] Copyright 2021, Springer Nature. d) PiFM images at a wave number of 1532 cm^{-1} (representing L8-BO) and 1648 cm^{-1} (representing PM6) and the line profiles along the white arrows to obtain the fibril width for the PM6:D18:L8-BO blended film. Reproduced with permission.[126] Copyright 2022, Springer Nature.

been regarded as one of the simplest and most effective strategies to optimize the active layer morphology. Solvent additives, e.g., DIO, are widely used in tuning donors and acceptor microstructure, especially for the crystallization of fullerenes.[132] Empirical evidence suggests that effective co-solvent systems typically involve a co-solvent with a higher boiling point than the main solvent and greater solubility for the fullerene derivative than for the polymer. In this way, the major concern of excessive aggregation in the fullerene phase was effectively circumvented.[133] However, the presence of residual solvent additives can easily become trapped in the active layer, altering its morphological evolution, particularly under light illumination, which negatively impacts long-term stability. In contrast, volatile solid additives could serve as promising candidates to enhance both efficiency and stability due to their volatility.[134] In NFA-OPVs, the design of novel solid additives relies on the properties of NFAs, where intermolecular end-group packing plays a key role in charge transport. This necessitates the development of targeted optimization strategies for additive design. In this example, Hou et al studied a series of volatile solid additives (SA-1 to SA-8) with a similar chemical structure to that of the end-groups of an A–D–A acceptor IT-4F to control its organization.[135] A morphology landscape was illustrated in **Figure 6a**: during the spin-coating process, SA-1 can be involved in π–π packing among IT-4F molecules. Thermal annealing could remove SA-1, leaving more freedom for the self-assembly of IT-4F and promoting a more ordered molecular

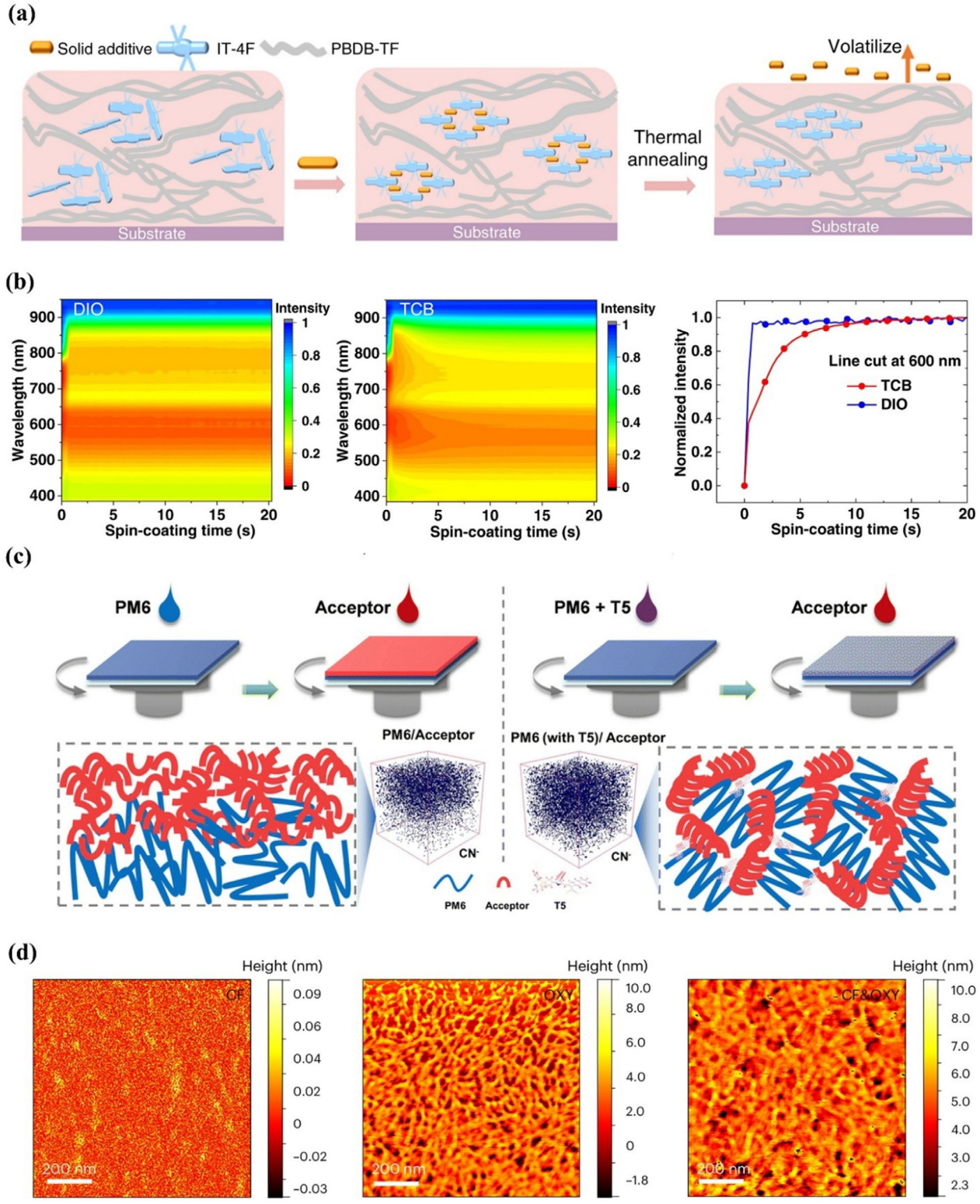

Figure 6. a) Schematic diagram of the working mechanism of Sas. Reproduced under the terms of the CC-BY Creative Commons Attribution 4.0 International license.[135] Copyright 2018, Springer Nature. b) Normalized in situ absorption intensity at the wavelength of 600 nm as a function of spin-coating time for PM6:Y6 blends with DIO and with TCB. Reproduced under the terms of the CC-BY Creative Commons Attribution 4.0 International license.[140] Copyright 2023, Springer Nature. c) Schematic illustration of active layer deposition of the LBL-OPV device. Reproduced with permission.[141] Copyright 2024, Royal Society of Chemistry. d) Tapping AFM-IR topography image for D18:2BTh-2F-C_2 blends at a wavenumber of 1700 cm^{-1} in different solvent combination conditions. Reproduced with permission.[144] Copyright 2024, Springer Nature.

arrangement. Notably, SA-1 selectively interacts with IT-4F rather than the polymer. This study guides researchers toward the understanding that the interaction between solid additives and organic materials is crucial in tailoring phase separation and morphology.[136–138] Song et al. found a π-backbone solid additive 1,3-dibromo-5-chlorobenzene (DBCl), to interact with the core unit of Y6.[139] During film formation, DBCl could act as the bridge to attract neighboring Y6 molecules due to the dipole interaction to form the intermediate phase, then heating would assist the removal of DBCl. Consequently, a more condensed molecular structure can be built, leading to a high FF of 80.2%. The studies above focus on the organization of acceptors by creating various non-covalent interactions with them. Fu et al. discovered a novel mechanism in which solid additives influence the crystallization process of both Y6 and the polymer through hydrogen bonding.[140] Specifically, 1,3,5-trichlorobenzene (TCB) can be easily removed during spin coating before thermal annealing, providing more flexibility for intermediate phase arrangement, such as initially enhancing and then relaxing molecular aggregation (as shown in Figure 6b). As a result, the excessive aggregation of non-fullerene acceptors was inhibited, leading to a significant reduction in non-radiative recombination loss to 0.190 eV. Different from the aggregation tuning of acceptors originating from additives, Li et al. introduced a novel non-volatile solid additive, T5, to modulate the packing properties and orientation within polymer domains during sequential deposition processes (Figure 6c).[141] In situ absorption spectroscopy revealed that T5 acts as an initiator, promoting the pre-aggregation of polymer chains and enhancing their long-range ordering. Excitingly, this enhanced packing of polymers can inhibit the non-radiation recombination pathways. Another scenario is the co-solvent strategy, which was developed during the fullerene era, and is also effective in controlling the domain and aggregation of organic materials, including both polymer and fullerenes, via affecting the crystallization dynamics.[142,143] Recently, Zeng et al. chose co-solvents, chloroform, and *o*-xylene, which evaporate at different temperatures and rates and have varying solubilities for D18.[144] As chloroform evaporates, D18 becomes supersaturated, leading to the polymer gelating through the formation of a fibrillar network. Subsequently, the evaporation of *o*-xylene accelerates the development of this network, arranging 2BTh-2F-C2 into pure, aggregated domains. Additionally, the use of the solid-state additive 1,4-diiodobenzene (DIB) was expected to enhance the self-organization of the materials. As evidenced by atomic force microscopy-based infrared microscopy (AFM-IR) measurements in Figure 6d, a bicontinuous morphology with distinctive fibril features could be formed. This concept works for materials that adopt different solubilities. The solvent design principles pave the way for an effective approach to morphology control in the processing of OPV layers. The performances of device engineering strategies are summarized in **Table 1**.

4. Stability of Active Layer

OPVs have made significant advancements in photovoltaic performance, yet many factors can limit the stability of OPVs during their commercialization, such as moisture, oxygen, light irradiation, and heating.[145] The introduction of NFAs into OPV devices has prompted a renewed evaluation of the degradation mechanisms under environmental conditions. Encapsulation technologies have proven effective in mitigating degradation caused by atmospheric moisture and oxygen.[146] From the materials perspective, light-induced instability primarily arises from photochemical and photophysical degradation within the active layer and charge transport layers. These degradation processes disrupt the conjugated molecular framework, resulting in increased energetic disorder, higher trap densities, and reduced charge carrier mobility.[147] For example, Zhang et al. utilized full-end-capping engineering to enhance the efficiency and stability of OPVs by eliminating unreacted terminal defects in the polymer donor structure.[148] A series of fully end-capped polymer donors—PM6-T, PM6-T-C1, PM6-T-C6, and PM6-T-C12—with varying end-capping groups were synthesized to achieve precise control over absorption characteristics, crystallinity, and donor–acceptor interactions. Notably, the PM6-T:Y6-based device not only achieved a record PCE of 18.4% but also exhibited improved storage, thermal, and photostability compared to conventional PM6:Y6-based OPVs. Even after 1200 hours of storage in a nitrogen glovebox, the PM6-T-based device retained 86% of its initial PCE. Regarding acceptor stability, NFA molecules can undergo photooxidation at the electron-deficient end groups and side chains, especially under illumination in the presence of oxygen or residual solvents.[149] Li et al. designed and synthesized an unfused-ring NFA, DF-PCIC, featuring excellent planarity through intramolecular non-covalent F···H interactions.[150] When compared to devices based on fused-core ITIC, the unfused DF-PCIC-based devices exhibited significantly enhanced thermal stability. This improvement can be attributed to the stabilized morphology resulting from intramolecular F···H non-covalent interactions. Compared to small-molecule acceptors, polymeric acceptors demonstrate superior morphological stability due to their higher molecular weights and restricted molecular diffusion. These intrinsic properties make all-polymer solar cells (all-PSCs) particularly advantageous for flexible and wearable electronics, where enhanced mechanical durability and long-term operational stability are crucial. Building upon PY-T-γ, Yu et al. further developed two linkage-substituted polymer acceptors, PY-V-γ and PY-2T-γ, for all-PSCs.[151] These acceptors replaced the thiophene linker unit with vinylene and bithiophene, respectively. As the linker size decreased, the backbone rigidity increased, leading to stronger conjugation and a more stable chain conformation in the order of PY-2T-γ < PY-T-γ < PY-V-γ. Consequently, devices based on these polymers exhibited enhanced stability under thermal aging and bending tests.

Morphological degradation, particularly phase separation, can significantly compromise the long-term stability of OPVs. Recent reports have claimed that the morphology degradation also affects the stability of solar cell devices, especially playing a key role in the initial degradation stage, e.g., burn-in behavior under heat or/and light. From the thermodynamic point of view, the as-cast optimized morphology in the active layer is usually away from the thermodynamic equilibrium point (metastable state) and can slowly evolve to the equilibrium state (stable state) after aging period. In addition, extrinsic degradation factors in the real world fasten this morphological evolution process, which presents fast degradation at the initial stage. When the morphology evolved close to the equilibrium, the rate of evolution can slow down then and present as the slow linear degradation. Valid strategies that

Table 1. Summary of device parameters via morphology control strategies.

Planar Structure	Donor/Acceptor	Solvents for donor/acceptor	V_{OC} [V]	J_{SC} [mA cm^{-2}]	FF [%]	PCE_{avg} (PCE_{max}) [%]	Refs.
	P3HT/$PC_{61}BM$	ODCB/DCM	0.63	8.2	66	3.5	[98]
	PTB7/ $PC_{61}BM$	CB/(2-CP+1-Butanol)	0.76	13.7	57	6	[100]
	P3HT/ $PC_{61}BM$	CF+EG/ DCM	0.639	10.17	52.72	3.43	[101]
	PTB7-TH/$PC_{71}BM$	/DCM+DCB	0.81	16.6	62.7	8.5 (8.6)	[102]
	PBDB-TFS1/IT-4F	CB/THF+o-DCB	0.90	20.3	71	13.0	[103]
	PM6/Y6-BO	CF/CF	0.847	26.2	77.5	16.9 (17.2)	[104]
	PM6/BO-4Cl+BTP-S2	CF/CF	0.861	27.14	78.04	18.03 (18.16)	[107]
	PM6/BTP-eC9+PY-IT	XY/XY	0.859	27.79	0.813	19.15 (19.41)	[153]
	D18/S9SBO-F:Y6-O	CB/CF	0.84	29.56	77.12	19.15	[111]
Multicomponent Strategy	Binary BHJ active layer	Third component	V_{OC} (V)	J_{SC} (mA/cm^2)	FF (%)	PCE_{avg} (PCE_{max}) (%)	Ref.
	PTB7:$PC_{71}BM$	PBDTT-SeDPP	0.69	18.7	67.4	8.7	[116]
	PDBT-T1: SdiPBI-Se	ITIC-Th	0.931	15.37	70.2	10.1	[118]
	J52:IT-M	IEICO	0.847	19.7	66.8	10.9 (11.1)	[120]
	PM6: ITCPTC	MeIC	0.981	18.42	78.2	13.83 (14.13)	[121]
	P3HT:IDTBR	IDFBR	1.03	17.2	60	11.0	[122]
	BTR:NITI	$PC_{71}BM$	0.94	19.50	73.83	13.20 (13.63)	[123]
	PM6:Y6	BTO: $PC_{71}BM$	0.85	27.12	75.75	17.30 (17.41)	[125]
	PM6:L8-BO	D18	0.896	26.7	81.9	19.3 (19.6)	[126]
	D18:L8-BO	Z8	0.92	27.2	80.8	19.8 (20.2)	[127]
	PM6:BTP-eC9	o-BTP-eC9	0.860	28.75	80.41	19.55 (19.88)	[128]
Solvent engineering	BHJ Active layer	Additive	V_{OC} (V)	J_{SC} (mA/cm^2)	FF (%)	PCE_{avg} (PCE_{max}) (%)	Ref.
	PCPDTBT:$PC_{71}BM$	DIO	0.61	15.73	53	5.12	[132]
	PBDB-TF:IT-4F	SA1	0.86	20.2	76	13.3(13.8)	[135]
	PM6:Y6	DBCl	0.85	25.8	78.5	16.9 (17.2)	[139]
	PM6:BTP-eC9	TCB	0.852	27.02	78.43	17.86 (18.06)	[140]
	PM6:Y6	T5/DCBB	0.840	28.35	79.31	18.83(18.89)	[141]
	D18:2BTh-2F-C2	DIB	0.913	26.71	77.98	18.71 (19.02)	[144]

stabilize or fix the morphological microstructure have been extensively explored, including using solid additives,[139] introducing third components,[152] establishing vertical phase separation,[153] and designing polymers acceptors.[154] For example, An et al. improved the device stability by controlling thermodynamic phase separation accelerated by thermal stresses.[155] They utilized two acceptor mixtures with varied thermal behaviors to reduce the melting point and enthalpy, thereby inhibiting the amorphous region from coarsening or aggregation. Eventually, an outstanding thermal stability of devices was achieved after 1400 h continuous heating under 85 °C. Similarly, Baran's group observed that the formation of a glassy state in the active layer materials suppressed configurational crystallization, leading to enhanced morphological stability.[122] Therefore, to improve the stability from the thermodynamic point of view, it is imperative to tune molecular interaction (e.g., miscibility) and glass transition properties of materials, which would govern the crystallization-induced phase separation evolution during the long-term aging processes.

5. Semitransparent OPVs

Semitransparent organic photovoltaics (ST-OPVs) have gained significant attention in recent years due to their potential applications in energy generation for BIPV, smart windows, and other transparent electronic devices.[156–159] Unlike traditional opaque solar cells, ST-OPVs require not only high PCE but also significant optical transparency in the visible spectrum, where average visible transmittance (AVT) is commonly used. Thus, the light utilization efficiency (LUE = PCE×AVT) has been proposed as a useful figure of merit to track the progress of ST-OPVs.[160–162] Other key factors to assess the performance of ST-OPVs include aesthetic and thermal insulation performance.

5.1. LUE

There is often a trade-off between AVT and PCE. The AVT value is determined by calculating the average value of transmittance of the transparent device in the visible light wavelength range (380–780 nm) based on the photonic response of the human eye. The AVT value of ST-OPVs can be calculated according to the following equation:

$$\mathrm{AVT} = \frac{\int_{380}^{740} T(\lambda) \times P(\lambda) \times AM1.5G(\lambda)\, d(\lambda)}{\int_{380}^{740} P(\lambda) \times AM1.5G(\lambda)\, d(\lambda)} \quad (1)$$

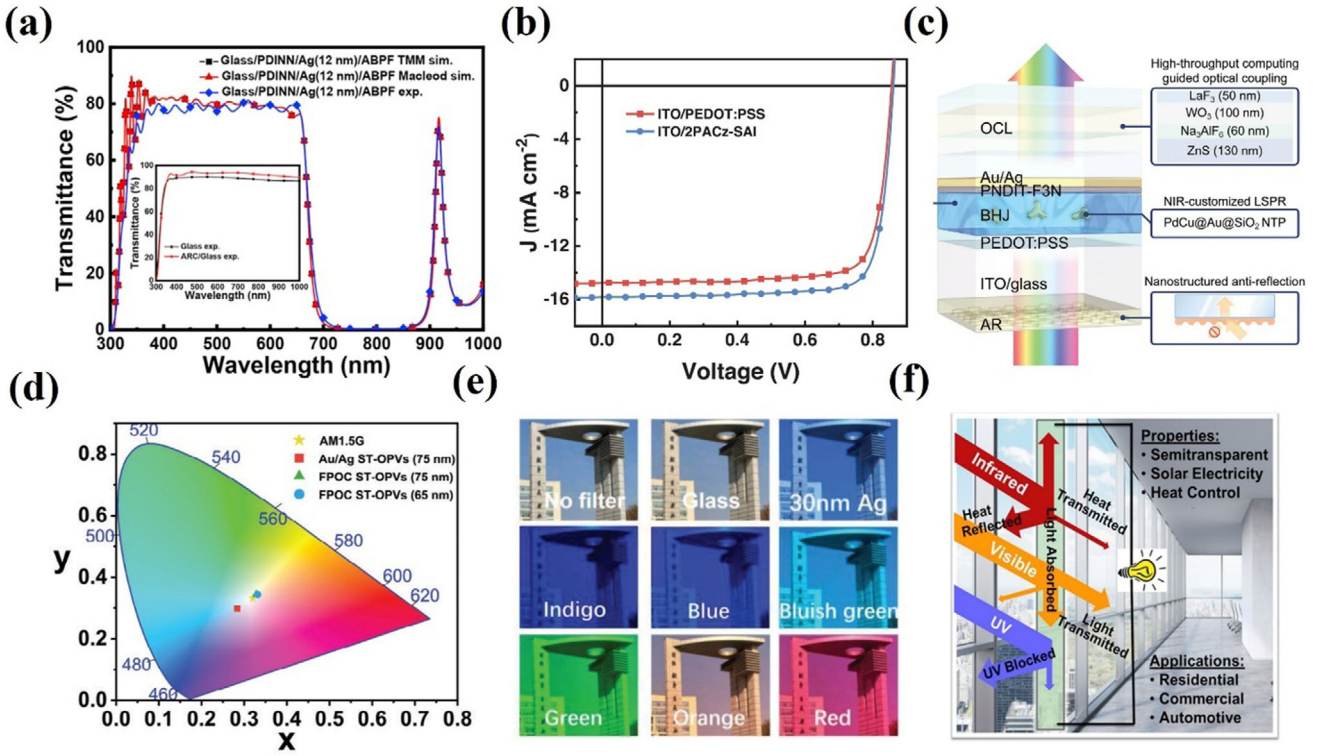

Figure 7. a) Transparent rear electrode via integrating an aperiodic bandpass filter. Reproduced with permission.[165] Copyright 2022, Cell Press. b) *J–V* curves under the strategy of a self-assembled interlayer for ST-OPVs. Reproduced with permission.[168] Copyright 2024, Wiley-VCH. c) The schematic diagram of ST-OPVs with a synergetic near-infrared light management. Reproduced with permission.[166] Copyright 2024, Wiley-VCH. d) The CIE 1931 chromaticity of neutral-color ST-OPVs. Reproduced with permission.[173] Copyright 2024, Wiley-VCH. e) The digital camera images of colorful ST-OPVs. Reproduced with permission.[180] Copyright 2023, Wiley-VCH. f) The schematic diagram of heat-insulating multifunctional ST-OPVs. Reproduced with permission.[181] Copyright 2018, Cell Press.

where $T(\lambda)$ is the transmission spectrum of ST-OPVs, $P(\lambda)$ is the photopic response of the human eye, and AM1.5G(λ) is the photon flux under AM 1.5G light illumination conditions.

A range of organic materials can be engineered for specific AVT, meeting the requirements of various applications.[36,163] With the development of NIR non-fullerene acceptors and optical design, the LUE value exceeds 5%.[164–169] For example, Liu et al. reported a superior transparent rear electrode for ST-OPVs via integrating an aperiodic bandpass filter with a total reflection in the near-infrared region (700–900 nm) (**Figure 7a**), delivering a record LUE of 5.35% with an excellent AVT of 46.79%.[165] Xu et al. have also reported a synergetic near-infrared light management for ST-OPVs and achieved a high PCE of 16.14% along with an AVT of 33.02%, resulting in a LUE of 5.33%, as shown in Figure 7c.[166] Achieving high PCE for opaque devices is also one of the effective ways to improve the ultimate LUE for ST-OPVs. Guan et al. have achieved an outstanding PCE of 20.17% by developing the strategy of a self-assembled interlayer, delivering a high LUE of 5.34% due to elevated absorbing selectivity, in which *J–V* curve is illustrated in Figure 7b.[168] Despite the PCEs of OPVs having been significantly improved, exceeding 20%, the advancements in ST-OPVs are still stagnant. One of the main reasons is that the polymer donor for highly efficient OPVs, for example, PM6, is highly overlapping with the visible wavelength range, resulting in a drastic decrease in the AVT. Reducing the donor ratio is also a commonly used method in optimizing ST-OPVs.[159]

5.2. Aesthetic

The aesthetics of ST-OPVs play a crucial role in their integration into modern architectural designs and urban landscapes, providing a visually appealing solution for application in windows or other BIPV.[170,171] The design flexibility of ST-OPVs allows for a variety of customization options, which can be manufactured in different colors, patterns, and transparencies to create unique, artistic facades for both functional energy generators and visually striking elements. The color rendering index (CRI) and Commission Internationale de L'Eclairage (CIE 1931) chromaticity coordinates are the main parameters to elevate the aesthetics of ST-OPVs.[172] The CRI approaching 100 means displaying the intrinsic color of the object. Recently, Yu et al. have reported high-performance neutral-color ST-OPVs by integrating an Ag/TeO_2/Ag/TeO_2-based Fabry–Perot resonant optical coating, delivering a superior CRI value of 99.23 (Figure 7d) with good angular insensitivity up to ±60°.[173] For colorful ST-OPVs, the parameter of CIE 1931 chromaticity coordinates is utilized to quantify their color appearance, which can be perceived by the human eye. Numerous optical structures, such as chromatic

plasmonic polarizers,[174] optical spacers,[175] 1D photonic crystals (1DPCs),[176] induced transmission filters,[177] and microcavity resonance color filters[178–180] have been investigated for chromatic ST-OPVs. Liu et al. developed a wide color gamut and high color purity for colorful ST-OPVs with a distinctive microcavity resonance color filter (CF) structure of silver/ bismuth(III) fluoride/silver (shown in Figure 7e)[180] Their ability to merge energy generation with aesthetic design opens up new possibilities for sustainable and visually compelling buildings.

5.3. Thermal Insulation

Since most ST-OPVs use thin silver (Ag) metal as the rear electrode, ST-OPVs exhibit a natural thermal insulation effect due to the high reflectivity of Ag in the infrared region. The NIR solar energy rejection (NIR-SER) has been defined to quantify the solar energy rejection of commonly used tinted window films.

$$NIR-SER=\frac{\int_{780}^{2500}\left[R\left(\lambda\right)+A\left(\lambda\right)\right]P_{AM1.5G}\left(\lambda\right)d\lambda}{\int_{780}^{2500}P_{AM1.5G}\left(\lambda\right)d\lambda} \quad (2)$$

where $R(\lambda)$, $A(\lambda)$, and $P_{\mathrm{AM\ 1.5G}}(\lambda)$ represent the reflectance, absorbance of the film, and the $P_{\mathrm{AM\ 1.5G}}$ photon flux solar power density spectrum (ASTM G173-03) at specific wavelengths, respectively. As shown in Figure 7f, Zhang et al. have reported heat-insulating multifunctional ST-OPVs with NIR-SER of over 80%.[181] Further coupled with an optical layer optimized through high-throughput optical modeling, an outstanding NIR-SER of over 95% for ST-OPVs can be achieved.[182] These capabilities of ST-OPVs offer great potential for efficiently utilizing spectrum-engineered solar photons, enabling both power generation and energy savings.

The operational stability of ST-OPVs is a critical factor in determining their commercial viability, especially for large-scale applications. Sun et al. reported large-area modules with a PCE of 11.28% for ST-OPVs.[183] These modules worked healthily under outdoor operation. Zhao et al. reported ST-OPVs achieving a PCE of 13.5% and an AVT of 21.5%, demonstrating remarkable operational stability by maintaining 84.8% of their performance after 1008 h of continuous illumination. Additionally, greenhouse studies indicate that ST-OPV roofs enhance both the survival rate and growth of crops.[184]

6. Conclusion and Perspective

This review highlighted the recent progress of OPVs in achieving efficiencies exceeding 20%, with a particular emphasis on materials development, especially the advancements in nonfullerene acceptors and donor materials. Additionally, we emphasize the critical role of precise morphology control through three main strategies: planar structure innovation, multicomponent strategies, and additive and solvent engineering. These strategies offer insights and optimization pathways that bridge morphology and device performance in OPVs. The review also explores the competitive and promising applications of TOPVs, focusing on active layer and transparent optical structure designs. However, despite these advancements, significant challenges and concerns remain to be addressed to further drive the commercialization of OPVs. Despite significant advancements in OPVs, several intrinsic limitations hinder their further development and commercialization. Addressing these challenges through innovative molecular design strategies is crucial for achieving higher efficiencies, improved stability, and scalable processing. Below, we outline key directions for future research in OPVs:

6.1. Molecule Design

1) AI-assisted molecular design and donor-acceptor combinations optimization. AI and machine learning can play a transformative role in accelerating the discovery of high-performance materials. By leveraging AI-driven algorithms, researchers can predict molecular properties, optimize D–A combinations, and identify materials with tailored energy levels, absorption spectra, and charge transport properties. This approach not only reduces experimental trial-and-error but also enables the design of materials with minimized energy losses and enhanced device performance. 2) Development of entirely new molecules with low energy loss. Energy loss, particularly non-radiative energy loss, remains one of the primary limitations for achieving efficiency breakthroughs in OPVs. It is essential to design new molecular structures with higher EQE_{EL} and PLQY than that of NFAs. By optimizing molecular structures to simultaneously minimize non-radiative losses while preserving efficient charge generation and transport. 3) Developing simple and efficient donor–acceptor materials to reduce synthesis costs. Non-fused NFAs and non-fused thiophene-based polymers have emerged as promising candidates due to their simplified synthesis, lower production costs, and enhanced stability. These materials also exhibit excellent solution processability, making them suitable for large-scale manufacturing. Future research should focus on optimizing their molecular structures to achieve a balance among efficiency, stability, and processability, paving the way for cost-effective and high-performance OPVs. 4) Molecular design aimed at enhancing dielectric properties. That is, to develop high dielectric constant and low binding energy of OPV materials to mitigate low dielectric constant and high binding energy. For example, this can be achieved by incorporating polar functional groups or designing molecules with intrinsic charge separation capabilities, which reduce exciton binding energy and improve charge generation efficiency.

6.2. Morphology Control

People cannot ignore the importance of precise control over the active layer morphology, e.g., crystallinity and phase separation, for advancing the efficiency of OPV devices. The morphology control involves both thermodynamic and non-equilibrium dynamic considerations, in which synergetic optimization strategies, involving thermal annealing, solvent additives, and solvent, and rational D/A pairing, are normally carried out together to achieve ideal continuous fibril nanostructure. Fullerenes involved active layer suffers from large domains with around hundreds of nanometers, while the NFAs, especially small molecules, could offer more flexibility for tailoring the phase separation

approaching the tens of nanometers, which is very close to the exciton diffusion length. Most recently, however, mixing between polymer and NFAs seems a big issue that pure domain is not sufficient for charge transport. Therefore, most recently, the crystallization rate-induced phase separation strategy seems to become a direction toward the so-called fibrillar structure—one is crystallized first to form a fibril and the other is arranged later, which would avoid too much mixing and thus undesired charge recombination. Additionally, increasing research efforts have focused on interfacial domains and phase separation near the electrode, where a p–i–n structure can provide relatively pure domains for efficient charge transport. Notably, the unclear correlation between microstructure and stability creates ambiguity in comprehensively evaluating the optimal morphology. To get deeper and novel structure and performance relationship, more morphology characterization techniques at multilength scale via both ex situ and in situ detection should be further explored to offer better morphology recognition in realistic film processing conditions, especially at the molecular and even atomic level.

Moreover, interface engineering, including the design of electron and hole transporting layers as well as device structures, deserves greater attention. Current state-of-the-art OPVs predominantly rely on the conventional structure incorporating PEDOT:PSS, which suffers from chemical instability during long-term operation. The inverted structure presents a promising alternative with high resilience to external stresses and greater stability potential;[185] however, it has received comparatively less attention. One of the major challenges lies in the presence of oxygen vacancies in ZnO, which can progressively degrade device performance through photooxidation processes. Therefore, mitigating these vacancies is essential to fully harness the potential of ZnO in enhancing the operational stability of OPV devices. Huang et al. proposed an innovative method for in situ acidized synthesis of ZnO.[186] They demonstrated that propionic acid groups could anchor onto the ZnO surface via coordination bonding, thereby suppressing the adsorption of oxygen species and water at oxygen vacancy sites. This inhibition effectively prevents the generation of superoxide and hydroxyl radicals, which would otherwise catalyze the degradation of PM6 and BTP-eC9. As a result, the devices exhibited remarkable stability, retaining 94.2% of their initial PCE after 8904 h of ambient storage without encapsulation under the ISOS-D-1 protocol, and 81.5% PCE retention after 7724 h of MPP tracking under the ISOS-L-1 protocol. Subsequently, Liu et al. adopted an effective approach by passivating ZnO defects using an inorganic layer, SiOxNy.[187] This passivation layer effectively mitigates oxygen vacancies through strong Zn—O—Si bonding, significantly enhancing the device's stability. The progress achieved in interfacial layer engineering of inverted OPVs offers a promising pathway toward the development of highly stable and efficient devices. Therefore, continued efforts and innovative strategies are essential to further advance the design of more efficient and robust transport layers. Additionally, innovations in device architecture—such as tandem OPVs—have pushed efficiencies beyond the Shockley–Queisser limit for single-junction devices. Tandem structures that stack complementary absorbing layers are expected to dominate future OPV research.

6.3. Potential Applications

Their semitransparent nature makes OPVs ideal for windows, glass facades, skylights, and other transparent surfaces, offering energy generation and aesthetic appeal. Research into new materials, optimized device architectures, and improved processing techniques are expected to push ST-OPV efficiencies (PCE and LUE) higher in the coming years. As manufacturing techniques improve, scaling the production of large-area ST-OPV modules will become more feasible, which will help accelerate the adoption of BIPV applications. Research in encapsulation technologies, as well as the development of more stable materials, is progressing rapidly to improve the long-term stability and durability of ST-OPVs. ST-OPVs with the abilities of power generation, energy-saving, and aesthetics will contribute to a more sustainable and energy-efficient future.

Acknowledgements

Y.Z. and H.X. contributed equally to this work. This work was supported by Research Grants Council of Hong Kong (project ID: C4005-22Y, C7018-20G), RGC Senior Research Fellowship Scheme (SRFS2223-5S01), the Hong Kong Polytechnic University: Sir Sze-yuen Chung Endowed Professorship Fund (8-8480), PRI (Q-CD7X), G-SAC5, Guangdong-Hong Kong-Macao Joint Laboratory for Photonic-Thermal-Electrical Energy Materials and Devices (GDSTC number 2019B121205001).

Conflict of Interest

The authors declare no conflict of interest.

Keywords

device engineering, morphology control, nonfullerene acceptors and donors, organic photovoltaic, semitransparent

Received: February 28, 2025
Revised: May 6, 2025
Published online:

[1] G. Li, R. Zhu, Y. Yang, *Nat. Photonics* **2012**, *6*, 153.
[2] C. Yan, S. Barlow, Z. Wang, H. Yan, A. K. Y. Jen, S. R. Marder, X. Zhan, *Nat. Rev. Mater.* **2018**, *3*, 18003.
[3] Y. Li, G. Xu, C. Cui, Y. Li, *Adv. Energy Mater.* **2018**, *8*, 1701791.
[4] J. You, L. Dou, K. Yoshimura, T. Kato, K. Ohya, T. Moriarty, K. Emery, C. C. Chen, J. Gao, G. Li, Y. Yang, *Nat. Commun.* **2013**, *4*, 1446.
[5] H. Yin, C. Yan, H. Hu, J. K. W. Ho, X. Zhan, G. Li, S. K. So, *Mater. Sci.Eng.: R: Rep.* **2020**, *140*, 100542.
[6] Z. Xu, S.-H. Li, L. Ma, G. Li, Y. Yang, *Appl. Phys. Lett.* **2007**, *91*, 092911.
[7] L. Zhan, S. Li, Y. Li, R. Sun, J. Min, Y. Chen, J. Fang, C. Q. Ma, G. Zhou, H. Zhu, L. Zuo, H. Qiu, S. Yin, H. Chen, *Adv. Energy Mater.* **2022**, *12*, 2201076.
[8] P. Bi, J. Wang, Y. Cui, J. Zhang, T. Zhang, Z. Chen, J. Qiao, J. Dai, S. Zhang, X. Hao, Z. Wei, J. Hou, *Adv. Mater.* **2023**, *35*, 2210865.
[9] C. Chen, L. Wang, W. Xia, K. Qiu, C. Guo, Z. Gan, J. Zhou, Y. Sun, D. Liu, W. Li, T. Wang, *Nat. Commun.* **2024**, *15*, 6865.
[10] R. Ma, H. Li, T. A. Dela Pena, H. Wang, C. Yan, P. Cheng, J. Wu, G. Li, *Natl. Sci. Rev.* **2024**, *11*, nwae384.

[11] A. Kumar, R. Devine, C. Mayberry, B. Lei, G. Li, Y. Yang, *Adv. Funct. Mater.* **2010**, *20*, 2729.
[12] C. W. Tang, *Appl. Phys. Lett.* **1986**, *48*, 183.
[13] M. Hiramoto, H. Fujiwara, M. Yokoyama, *J. Appl. Phys.* **1992**, *72*, 3781.
[14] G. Yu, J. Gao, J. C. Hummelen, F. Wudl, A. J. Heeger, *Science* **1995**, *270*, 1789.
[15] J. J. M. Halls, C. A. Walsh, N. C. Greenham, E. A. Marseglia, R. H. Friend, S. C. Morattlt, A. B. Holmes, *Nature* **1995**, *376*, 498.
[16] J. Hou, O. Inganas, R. H. Friend, F. Gao, *Nat. Mater.* **2018**, *17*, 119.
[17] V. Coropceanu, X.-K. Chen, T. Wang, Z. Zheng, J.-L. Brédas, *Nat. Rev. Mater.* **2019**, *4*, 689.
[18] X. K. Chen, V. Coropceanu, J. L. Bredas, *Nat. Commun.* **2018**, *9*, 5295.
[19] J. Liu, S. Chen, D. Qian, B. Gautam, G. Yang, J. Zhao, J. Bergqvist, F. Zhang, W. Ma, H. Ade, O. Inganäs, K. Gundogdu, F. Gao, H. Yan, *Nat. Energy* **2016**, *1*, 16089.
[20] J. Yuan, T. Huang, P. Cheng, Y. Zou, H. Zhang, J. L. Yang, S. Y. Chang, Z. Zhang, W. Huang, R. Wang, D. Meng, F. Gao, Y. Yang, *Nat. Commun.* **2019**, *10*, 570.
[21] G. Li, V. Shrotriya, J. Huang, Y. Yao, T. Moriarty, K. Emery, Y. Yang, *Nat. Mater.* **2005**, *4*, 864.
[22] L. Dou, J. You, J. Yang, C.-C. Chen, Y. He, S. Murase, T. Moriarty, K. Emery, G. Li, Y. Yang, *Nat. Photonics* **2012**, *6*, 180.
[23] J. Wang, S. Xie, D. Zhang, R. Wang, Z. Zheng, H. Zhou, Y. Zhang, *J. Mater. Chem. A* **2018**, *6*, 19934.
[24] Y. Zhao, Y. Zhu, H.-W. Cheng, R. Zheng, D. Meng, Y. Yang, *Mater. Today Energy* **2021**, *22*, 100852.
[25] H. Xia, X. Xu, J. Guo, C. Qian, K. Zhang, M. Zhu, B. Zhang, W. Peng, Q. Peng, W. Zhu, *Dyes Pigm.* **2021**, *186*, 108950.
[26] Y. Cui, C. Yang, H. Yao, J. Zhu, Y. Wang, G. Jia, F. Gao, J. Hou, *Adv. Mater.* **2017**, *29*, 1703080.
[27] W. Li, L. Ye, S. Li, H. Yao, H. Ade, J. Hou, *Adv. Mater.* **2018**, *30*, 1707170.
[28] H. Xia, X. Xu, C. Qian, J. Guo, J. Zhao, K. Zhang, H. Tan, Q. Peng, W. Zhu, *ACS Appl. Energy Mater.* **2022**, *5*, 3146.
[29] M. Zhang, X. Guo, W. Ma, S. Zhang, L. Huo, H. Ade, J. Hou, *Adv. Mater.* **2014**, *26*, 2089.
[30] T. Liu, R. Ma, Z. Luo, Y. Guo, G. Zhang, Y. Xiao, T. Yang, Y. Chen, G. Li, Y. Yi, *Energy Environ. Sci.* **2020**, *13*, 2115.
[31] C. Zhou, Y. Liang, F. Liu, C. Sun, X. Huang, Z. Xie, F. Huang, J. Roncali, T. P. Russell, Y. Cao, *Adv. Funct. Mater.* **2014**, *24*, 7538.
[32] L. Yuan, K. Lu, B. Xia, J. Zhang, Z. Wang, D. Deng, J. Fang, L. Zhu, Z. Wei, *Adv. Mater.* **2016**, *28*, 5980.
[33] A. Mishra, G. D. Sharma, *Angew. Chem., Int. Ed.* **2023**, *135*, 202219245.
[34] X. Guo, Q. Liao, E. F. Manley, Z. Wu, Y. Wang, W. Wang, T. Yang, Y.-E. Shin, X. Cheng, Y. Liang, *Chem. Mater.* **2016**, *28*, 2449.
[35] Q. Yue, W. Liu, X. Zhu, *J. Am. Chem. Soc.* **2020**, *142*, 11613.
[36] F. Liu, Z. Zhou, C. Zhang, J. Zhang, Q. Hu, T. Vergote, F. Liu, T. P. Russell, X. Zhu, *Adv. Mater.* **2017**, *29*, 1606574.
[37] K. Zhou, K. Xian, L. Ye, *InfoMat* **2022**, *4*, 12270.
[38] C. Cui, Y. Li, *Aggregate* **2021**, *2*, 31.
[39] P. E. Hartnett, H. R. Matte, N. D. Eastham, N. E. Jackson, Y. Wu, L. X. Chen, M. A. Ratner, R. P. Chang, M. C. Hersam, M. R. Wasielewski, *Chem. Sci.* **2016**, *7*, 3543.
[40] H. Zhong, C.-H. Wu, C.-Z. Li, J. Carpenter, C.-C. Chueh, J.-Y. Chen, H. Ade, A. K.-Y. Jen, *Adv. Mater* **2016**, *28*, 951.
[41] Y. Zhong, M. T. Trinh, R. Chen, G. E. Purdum, P. P. Khlyabich, M. Sezen, S. Oh, H. Zhu, B. Fowler, B. Zhang, *Nat. Commun.* **2015**, *6*, 8242.
[42] K. Jiang, Q. Wei, J. Y. L. Lai, Z. Peng, H. K. Kim, J. Yuan, L. Ye, H. Ade, Y. Zou, H. Yan, *Joule* **2019**, *3*, 3020.
[43] C. Xiao, X. Wang, T. Zhong, R. Zhou, X. Zheng, Y. Liu, T. Hu, Y. Luo, F. Sun, B. Xiao, *Adv. Sci.* **2023**, *10*, 2206580.
[44] J. Zhang, F. Bai, I. Angunawela, X. Xu, S. Luo, C. Li, G. Chai, H. Yu, Y. Chen, H. Hu, *Adv. Energy Mater.* **2021**, *11*, 2102596.
[45] H. Lu, W. Liu, H. Jin, H. Huang, Z. Tang, Z. Bo, *Adv. Funct. Mater.* **2022**, *32*, 2107756.
[46] Q. He, P. Ufimkin, F. Aniés, X. Hu, P. Kafourou, M. Rimmele, C. L. Rapley, B. Ding, *SusMat* **2022**, *2*, 591.
[47] J. Hai, Y. Song, L. Li, X. Liu, X. Shi, Z. Huang, G. Qian, Z. Lu, J. Yu, H. Hu, *Adv. Funct. Mater.* **2023**, *33*, 2213429.
[48] H. Huang, Q. Guo, S. Feng, C. e. Zhang, Z. Bi, W. Xue, J. Yang, J. Song, C. Li, X. Xu, Z. Tang, W. Ma, Z. Bo, *Nat. Commun.* **2019**, *10*, 3038.
[49] M. Yang, W. Wei, X. Zhou, Z. Wang, C. Duan, *Energy Mater.* **2022**, *1*, 100008.
[50] Q. Shen, C. He, S. Li, L. Zuo, M. Shi, H. Chen, *Acc. Mater. Res.* **2022**, *3*, 644.
[51] X. Guo, Q. Fan, J. Wu, G. Li, Z. Peng, W. Su, J. Lin, L. Hou, Y. Qin, H. Ade, L. Ye, M. Zhang, Y. Li, *Angew. Chem., Int. Ed.* **2020**, *60*, 2322.
[52] B. Li, X. Yang, S. Li, J. Yuan, *Energy Environ. Sci.* **2023**, *16*, 723.
[53] Y. Cheng, Q. Mao, C. Zhou, X. Huang, J. Liu, J. Deng, Z. Sun, S. Jeong, Y. Cho, Y. Zhang, B. Huang, F. Wu, C. Yang, L. Chen, *Angew. Chem., Int. Ed.* **2023**, *62*.
[54] Y. Wang, D. Qian, Y. Cui, H. Zhang, J. Hou, K. Vandewal, T. Kirchartz, F. Gao, *Adv. Energy Mater.* **2018**, *8*, 1801352.
[55] H. Xia, Y. Zhang, K. Liu, W. Deng, M. Zhu, H. Tan, P. W. K. Fong, H. Liu, X. Xia, M. Zhang, T. A. Dela Peña, R. Ma, M. Li, J. Wu, Y. Lang, J. Fu, W.-Y. Wong, X. Lu, W. Zhu, G. Li, *Energy Environ. Sci.* **2023**, *16*, 6078.
[56] J. Yuan, C. Zhang, H. Chen, C. Zhu, S. H. Cheung, B. Qiu, F. Cai, Q. Wei, W. Liu, H. Yin, R. Zhang, J. Zhang, Y. Liu, H. Zhang, W. Liu, H. Peng, J. Yang, L. Meng, F. Gao, S. So, Y. Li, Y. Zou, *Sci. China Chem.* **2020**, *63*, 1159.
[57] Z. Chen, T. Wang, Z. Wen, P. Lu, W. Qin, H. Yin, X.-T. Hao, *ACS Energy Lett.* **2021**, *6*, 3203.
[58] Y. Shi, Y. Chang, K. Lu, Z. Chen, J. Zhang, Y. Yan, D. Qiu, Y. Liu, M. A. Adil, W. Ma, X. Hao, L. Zhu, Z. Wei, *Nat. Commun.* **2022**, *13*, 3256.
[59] Y. Jiang, Y. Li, F. Liu, W. Wang, W. Su, W. Liu, S. Liu, W. Zhang, J. Hou, S. Xu, *Nat. Commun.* **2023**, *14*, 5079.
[60] B. C. Thompson, J. M. J. Fréchet, *Angew. Chem., Int. Ed.* **2007**, *47*, 58.
[61] L. M. Chen, Z. Hong, G. Li, Y. Yang, *Adv. Mater.* **2009**, *21*, 1434.
[62] F. Liu, T. Hou, X. Xu, L. Sun, J. Zhou, X. Zhao, S. Zhang, *Macromol. Rapid Comm.* **2017**, *39*, 1700555.
[63] C. B. Nielsen, S. Holliday, H.-Y. Chen, S. J. Cryer, I. McCulloch, *Acc. Chem. Res.* **2015**, *48*, 2803.
[64] G. Zhao, Y. He, Z. Xu, J. Hou, M. Zhang, J. Min, H. Y. Chen, M. Ye, Z. Hong, Y. Yang, Y. Li, *Adv. Funct. Mater.* **2010**, *20*, 1480.
[65] Y.-Y. Lai, Y.-J. Cheng, C.-S. Hsu, *Energy Environ. Sci.* **2014**, *7*, 1866.
[66] P. Cheng, G. Li, X. Zhan, Y. Yang, *Nat. Photonics* **2018**, *12*, 131.
[67] W. Liu, X. Xu, J. Yuan, M. Leclerc, Y. Zou, Y. Li, *ACS Energy Lett.* **2021**, *6*, 598.
[68] Y. Lin, J. Wang, Z. G. Zhang, H. Bai, Y. Li, D. Zhu, X. Zhan, *Adv. Mater.* **2015**, *27*, 1170.
[69] G. Zhang, J. Zhao, P. C. Y. Chow, K. Jiang, J. Zhang, Z. Zhu, J. Zhang, F. Huang, H. Yan, *Chem. Rev.* **2018**, *118*, 3447.
[70] J. Yuan, Y. Zhang, L. Zhou, G. Zhang, H.-L. Yip, T.-K. Lau, X. Lu, C. Zhu, H. Peng, P. A. Johnson, M. Leclerc, Y. Cao, J. Ulanski, Y. Li, Y. Zou, *Joule* **2019**, *3*, 1140.
[71] Y. Cui, H. Yao, J. Zhang, T. Zhang, Y. Wang, L. Hong, K. Xian, B. Xu, S. Zhang, J. Peng, Z. Wei, F. Gao, J. Hou, *Nat. Commun.* **2019**, *10*, 2515.
[72] Y. Cui, H. Yao, J. Zhang, K. Xian, T. Zhang, L. Hong, Y. Wang, Y. Xu, K. Ma, C. An, C. He, Z. Wei, F. Gao, J. Hou, *Adv. Mater.* **2020**, *32*, 1908205.

[73] C. Li, J. Zhou, J. Song, J. Xu, H. Zhang, X. Zhang, J. Guo, L. Zhu, D. Wei, G. Han, J. Min, Y. Zhang, Z. Xie, Y. Yi, H. Yan, F. Gao, F. Liu, Y. Sun, *Nat. Energy* **2021**, *6*, 605.
[74] Y. Yang, Z.-G. Zhang, H. Bin, S. Chen, L. Gao, L. Xue, C. Yang, Y. Li, *J. Am. Chem. Soc.* **2016**, *138*, 15011.
[75] D. Yuk, M. H. Jee, C. W. Koh, W. W. Park, H. S. Ryu, D. Lee, S. Cho, S. Rasool, S. Park, O. H. Kwon, J. Y. Kim, H. Y. Woo, *Small* **2022**, *19*, 2206547.
[76] W. Zhu, A. P. Spencer, S. Mukherjee, J. M. Alzola, V. K. Sangwan, S. H. Amsterdam, S. M. Swick, L. O. Jones, M. C. Heiber, A. A. Herzing, G. Li, C. L. Stern, D. M. DeLongchamp, K. L. Kohlstedt, M. C. Hersam, G. C. Schatz, M. R. Wasielewski, L. X. Chen, A. Facchetti, T. J. Marks, *J. Am. Chem. Soc.* **2020**, *142*, 14532.
[77] H. Chen, Y. Zou, H. Liang, T. He, X. Xu, Y. Zhang, Z. Ma, J. Wang, M. Zhang, Q. Li, C. Li, G. Long, X. Wan, Z. Yao, Y. Chen, *Sci. China Chem.* **2022**, *65*, 1362.
[78] Y. Sun, L. Wang, C. Guo, J. Xiao, C. Liu, C. Chen, W. Xia, Z. Gan, J. Cheng, J. Zhou, Z. Chen, J. Zhou, D. Liu, T. Wang, W. Li, *J. Am. Chem. Soc.* **2024**, *146*, 12011.
[79] D. He, F. Zhao, C. Wang, Y. Lin, *Adv. Funct. Mater.* **2022**, *32*, 2111855.
[80] X. Li, X. Kong, G. Sun, Y. Li, *eScience* **2023**, *3*, 100171.
[81] D. Qian, L. Ye, M. Zhang, Y. Liang, L. Li, Y. Huang, X. Guo, S. Zhang, Z. a. Tan, J. Hou, *Macromolecules* **2012**, *45*, 9611.
[82] M. Zhang, X. Guo, W. Ma, H. Ade, J. Hou, *Adv. Mater.* **2015**, *27*, 4655.
[83] R. Ma, T. Liu, Z. Luo, Q. Guo, Y. Xiao, Y. Chen, X. Li, S. Luo, X. Lu, M. Zhang, *Sci. China Chem.* **2020**, *63*, 325.
[84] Q. Liu, Y. Jiang, K. Jin, J. Qin, J. Xu, W. Li, J. Xiong, J. Liu, Z. Xiao, K. Sun, *Sci. Bull.* **2020**, *65*, 272.
[85] C. Sun, F. Pan, H. Bin, J. Zhang, L. Xue, B. Qiu, Z. Wei, Z.-G. Zhang, Y. Li, *Nat. Commun.* **2018**, *9*, 743.
[86] Y. Jiang, K. Jin, X. Chen, Z. Xiao, X. Zhang, L. Ding, *J. Semicond* **2021**, *42*, 070501.
[87] H. Ning, Q. Jiang, P. Han, M. Lin, G. Zhang, J. Chen, H. Chen, S. Zeng, J. Gao, J. Liu, *Energy Environ. Sci.* **2021**, *14*, 5919.
[88] K. Sun, Z. Xiao, S. Lu, W. Zajaczkowski, W. Pisula, E. Hanssen, J. M. White, R. M. Williamson, J. Subbiah, J. Ouyang, *Nat. Commun.* **2015**, *6*, 6013.
[89] H. Chen, D. Hu, Q. Yang, J. Gao, J. Fu, K. Yang, H. He, S. Chen, Z. Kan, T. Duan, *Joule* **2019**, *3*, 3034.
[90] Z. Li, X. Wang, N. Zheng, A. Saparbaev, J. Zhang, C. Xiao, S. Lei, X. Zheng, M. Zhang, Y. Li, *Energy Environ. Sci.* **2022**, *15*, 4338.
[91] K. Gao, S. B. Jo, X. Shi, L. Nian, M. Zhang, Y. Kan, F. Lin, B. Kan, B. Xu, Q. Rong, *Adv. Mater.* **2019**, *31*, 1807842.
[92] B. Kan, M. Li, Q. Zhang, F. Liu, X. Wan, Y. Wang, W. Ni, G. Long, X. Yang, H. Feng, *J. Am. Chem. Soc.* **2015**, *137*, 3886.
[93] L. Yang, S. Zhang, C. He, J. Zhang, H. Yao, Y. Yang, Y. Zhang, W. Zhao, J. Hou, *J. Am. Chem. Soc.* **2017**, *139*, 1958.
[94] L. Yang, S. Zhang, C. He, J. Zhang, Y. Yang, J. Zhu, Y. Cui, W. Zhao, H. Zhang, Y. Zhang, *Chem. Mater.* **2018**, *30*, 2129.
[95] H. Xia, R. Ma, R. Hao, C. Qian, P. W. Fong, Y. Zhang, K. Liu, M. Zhang, T. A. D. Peña, H. T. Chandran, *Nano Energy* **2025**, *134*, 110549.
[96] H. Chen, Y. Huang, R. Zhang, H. Mou, J. Ding, J. Zhou, Z. Wang, H. Li, W. Chen, J. Zhu, Q. Cheng, H. Gu, X. Wu, T. Zhang, Y. Wang, H. Zhu, Z. Xie, F. Gao, Y. Li, Y. Li, *Nat. Mater.* **2025**, *24*, 444.
[97] X. Xu, W. Jing, H. Meng, Y. Guo, L. Yu, R. Li, Q. Peng, *Adv. Mater.* **2023**, *35*, 2208997.
[98] A. L. Ayzner, C. J. Tassone, S. H. Tolbert, B. J. Schwartz, *J. Phys. Chem. C* **2009**, *113*, 20050.
[99] A. L. Ayzner, S. C. Doan, B. Tremolet de Villers, B. J. Schwartz, *J. Phys. Chem. Lett.* **2012**, *3*, 2281.
[100] J. C. Aguirre, S. A. Hawks, A. S. Ferreira, P. Yee, S. Subramaniyan, S. A. Jenekhe, S. H. Tolbert, B. J. Schwartz, *Adv. Energy Mater.* **2015**, *5*, 1402020.
[101] D. H. Lee, Y. Michael Yang, J. You, E. Richard, G. Li, *Nanotechnology* **2014**, *25*, 295401.
[102] P. Cheng, C. Yan, Y. Wu, S. Dai, W. Ma, X. Zhan, *J. Mater. Chem. C* **2016**, *4*, 8086.
[103] Y. Cui, S. Zhang, N. Liang, J. Kong, C. Yang, H. Yao, L. Ma, J. Hou, *Adv. Mater.* **2018**, *30*, 1802499.
[104] H. Fu, W. Gao, Y. Li, F. Lin, X. Wu, J. H. Son, J. Luo, H. Y. Woo, Z. Zhu, A. K.-Y. Jen, *Small Methods* **2020**, *4*, 2000687.
[105] Q. Li, L.-M. Wang, S. Liu, L. Guo, S. Dong, G. Ma, Z. Cao, X. Zhan, X. Gu, T. Zhu, Y.-P. Cai, F. Huang, *ACS Energy Lett.* **2020**, 3637.
[106] R. Yu, G. Wu, Y. Cui, X. Wei, L. Hong, T. Zhang, C. Zou, S. Hu, J. Hou, Z. Tan, *Small* **2021**, *17*, 2103497.
[107] L. Zhan, S. Li, X. Xia, Y. Li, X. Lu, L. Zuo, M. Shi, H. Chen, *Adv. Mater.* **2021**, *33*, 2007231.
[108] S. Dong, K. Zhang, B. Xie, J. Xiao, H.-L. Yip, H. Yan, F. Huang, Y. Cao, *Adv. Energy Mater.* **2019**, *9*, 1802832.
[109] R. Sun, Q. Wu, J. Guo, T. Wang, Y. Wu, B. Qiu, Z. Luo, W. Yang, Z. Hu, J. Guo, M. Shi, C. Yang, F. Huang, Y. Li, J. Min, *Joule* **2020**, *4*, 407.
[110] Y. Zhang, K. Liu, J. Huang, X. Xia, J. Cao, G. Zhao, P. W. K. Fong, Y. Zhu, F. Yan, Y. Yang, X. Lu, G. Li, *Nat. Commun.* **2021**, *12*, 4815.
[111] K. Jiang, J. Zhang, C. Zhong, F. R. Lin, F. Qi, Q. Li, Z. Peng, W. Kaminsky, S.-H. Jang, J. Yu, X. Deng, H. Hu, D. Shen, F. Gao, H. Ade, M. Xiao, C. Zhang, A. K. Y. Jen, *Nat. Energy* **2022**, *7*, 1076.
[112] M. Koppe, H.-J. Egelhaaf, G. Dennler, M. C. Scharber, C. J. Brabec, P. Schilinsky, C. N. Hoth, *Adv. Funct. Mater.* **2010**, *20*, 338.
[113] M. Günther, N. Kazerouni, D. Blätte, J. D. Perea, B. C. Thompson, T. Ameri, *Nat. Rev. Mater.* **2023**, *8*, 456.
[114] P. P. Khlyabich, B. Burkhart, B. C. Thompson, *J. Am. Chem. Soc.* **2011**, *133*, 14534.
[115] L. Yang, H. Zhou, S. C. Price, W. You, *J. Am. Chem. Soc.* **2012**, *134*, 5432.
[116] Y. Yang, W. Chen, L. Dou, W.-H. Chang, H.-S. Duan, B. Bob, G. Li, Y. Yang, *Nat. Photonics* **2015**, *9*, 190.
[117] P. P. Khlyabich, A. E. Rudenko, B. C. Thompson, Y.-L. Loo, *Adv. Funct. Mater.* **2015**, *25*, 5557.
[118] T. Liu, Y. Guo, Y. Yi, L. Huo, X. Xue, X. Sun, H. Fu, W. Xiong, D. Meng, Z. Wang, F. Liu, T. P. Russell, Y. Sun, *Adv. Mater.* **2016**, *28*, 10008.
[119] H. B. Naveed, W. Ma, *Joule* **2018**, *2*, 621.
[120] R. Yu, S. Zhang, H. Yao, B. Guo, S. Li, H. Zhang, M. Zhang, J. Hou, *Adv. Mater.* **2017**, *29*, 1700437.
[121] T. Liu, Z. Luo, Q. Fan, G. Zhang, L. Zhang, W. Gao, X. Guo, W. Ma, M. Zhang, C. Yang, Y. Li, H. Yan, *Energy Environ. Sci.* **2018**, *11*, 3275.
[122] D. Baran, R. S. Ashraf, D. A. Hanifi, M. Abdelsamie, N. Gasparini, J. A. Rohr, S. Holliday, A. Wadsworth, S. Lockett, M. Neophytou, C. J. Emmott, J. Nelson, C. J. Brabec, A. Amassian, A. Salleo, T. Kirchartz, J. R. Durrant, I. McCulloch, *Nat. Mater.* **2017**, *16*, 363.
[123] Z. Zhou, S. Xu, J. Song, Y. Jin, Q. Yue, Y. Qian, F. Liu, F. Zhang, X. Zhu, *Nat. Energy* **2018**, *3*, 952.
[124] R. Yu, H. Yao, Y. Cui, L. Hong, C. He, J. Hou, *Adv. Mater.* **2019**, *31*, 1902302.
[125] H. Chen, R. Zhang, X. Chen, G. Zeng, L. Kobera, S. Abbrent, B. Zhang, W. Chen, G. Xu, J. Oh, S.-H. Kang, S. Chen, C. Yang, J. Brus, J. Hou, F. Gao, Y. Li, Y. Li, *Nat. Energy* **2021**, *6*, 1045.
[126] L. Zhu, M. Zhang, J. Xu, C. Li, J. Yan, G. Zhou, W. Zhong, T. Hao, J. Song, X. Xue, Z. Zhou, R. Zeng, H. Zhu, C.-C. Chen, R. C. I. MacKenzie, Y. Zou, J. Nelson, Y. Zhang, Y. Sun, F. Liu, *Nat. Mater.* **2022**, *21*, 656.
[127] Y. Jiang, S. Sun, R. Xu, F. Liu, X. Miao, G. Ran, K. Liu, Y. Yi, W. Zhang, X. Zhu, *Nat. Energy* **2024**, *9*, 975.
[128] J. Fu, Q. Yang, P. Huang, S. Chung, K. Cho, Z. Kan, H. Liu, X. Lu, Y. Lang, H. Lai, F. He, P. W. K. Fong, S. Lu, Y. Yang, Z. Xiao, G. Li, *Nat. Commun.* **2024**, *15*, 1830.

[129] G. Zhang, X. K. Chen, J. Xiao, P. C. Y. Chow, M. Ren, G. Kupgan, X. Jiao, C. C. S. Chan, X. Du, R. Xia, Z. Chen, J. Yuan, Y. Zhang, S. Zhang, Y. Liu, Y. Zou, H. Yan, K. S. Wong, V. Coropceanu, N. Li, C. J. Brabec, J. L. Bredas, H. L. Yip, Y. Cao, *Nat. Commun.* **2020**, *11*, 3943.
[130] Y. Cui, Y. Xu, H. Yao, P. Bi, L. Hong, J. Zhang, Y. Zu, T. Zhang, J. Qin, J. Ren, Z. Chen, C. He, X. Hao, Z. Wei, J. Hou, *Adv. Mater.* **2021**, *33*, 2102420.
[131] P. Bi, S. Zhang, Z. Chen, Y. Xu, Y. Cui, T. Zhang, J. Ren, J. Qin, L. Hong, X. Hao, J. Hou, *Joule* **2021**, *5*, 2408.
[132] J. K. Lee, W. Ma, C. J. Brabec, J. Yuen, J. S. Moon, J. Y. Kim, K. Lee, G. C. Bazan, A. J. Heeger, *J. Am. Chem. Soc.* **2008**, *130*, 3619.
[133] G. J. Hedley, A. J. Ward, A. Alekseev, C. T. Howells, E. R. Martins, L. A. Serrano, G. Cooke, A. Ruseckas, I. D. Samuel, *Nat. Commun.* **2013**, *4*, 2867.
[134] N. Li, C. J. Brabec, *Energy Environ. Sci.* **2015**, *8*, 2902.
[135] R. Yu, H. Yao, L. Hong, Y. Qin, J. Zhu, Y. Cui, S. Li, J. Hou, *Nat. Commun.* **2018**, *9*, 4645.
[136] S. Bao, H. Yang, H. Fan, J. Zhang, Z. Wei, C. Cui, Y. Li, *Adv. Mater.* **2021**, *33*, 2105301.
[137] J. Wang, Y. Wang, P. Bi, Z. Chen, J. Qiao, J. Li, W. Wang, Z. Zheng, S. Zhang, X. Hao, J. Hou, *Adv. Mater.* **2023**, *35*, 2301583.
[138] L. Chen, J. Yi, R. Ma, L. Ding, T. A. Dela Pena, H. Liu, J. Chen, C. Zhang, C. Zhao, W. Lu, Q. Wei, B. Zhao, H. Hu, J. Wu, Z. Ma, X. Lu, M. Li, G. Zhang, G. Li, H. Yan, *Adv. Mater.* **2023**, *35*, 2301231.
[139] X. Song, K. Zhang, R. Guo, K. Sun, Z. Zhou, S. Huang, L. Huber, M. Reus, J. Zhou, M. Schwartzkopf, S. V. Roth, W. Liu, Y. Liu, W. Zhu, P. Muller-Buschbaum, *Adv. Mater.* **2022**, *34*, 2200907.
[140] J. Fu, P. W. K. Fong, H. Liu, C.-S. Huang, X. Lu, S. Lu, M. Abdelsamie, T. Kodalle, C. M. Sutter-Fella, Y. Yang, G. Li, *Nat. Commun.* **2023**, *14*, 1760.
[141] Z. Li, L. Zhan, H. Qiu, X. Sun, H. Hu, R. Gui, H. Yin, R. Sun, J. Min, J. Yu, W. Fu, W. Qiu, Z.-X. Liu, S. Yin, H. Chen, *Energy Environ. Sci.* **2024**, *17*, 8293.
[142] Y. Yao, J. Hou, Z. Xu, G. Li, Y. Yang, *Adv. Funct. Mater.* **2008**, *18*, 1783.
[143] J. J. van Franeker, M. Turbiez, W. Li, M. M. Wienk, R. A. Janssen, *Nat. Commun.* **2015**, *6*, 6229.
[144] R. Zeng, M. Zhang, X. Wang, L. Zhu, B. Hao, W. Zhong, G. Zhou, J. Deng, S. Tan, J. Zhuang, F. Han, A. Zhang, Z. Zhou, X. Xue, S. Xu, J. Xu, Y. Liu, H. Lu, X. Wu, C. Wang, Z. Fink, T. P. Russell, H. Jing, Y. Zhang, Z. Bo, F. Liu, *Nat. Energy* **2024**, *9*, 1117.
[145] P. Cheng, X. Zhan, *Chem. Soc. Rev.* **2016**, *45*, 2544.
[146] S. Song, J. Lu, W. Ye, B. Zhang, X. Liu, G. Xing, S. Zhang, *Sci. China Chem.* **2021**, *64*, 1441.
[147] H. Liu, Y. Li, S. Xu, Y. Zhou, Z. a. Li, *Adv. Funct. Mater.* **2021**, *31*, 2106735.
[148] Y. Zhang, J. Deng, Q. Mao, S. Y. Jeong, X. Huang, L. Zhang, B. Lee, B. Huang, H. Y. Woo, C. Yang, *Chem. Eng. J.* **2023**, *457*, 141343.
[149] H. Xu, J. Han, S. Chen, Y. Liu, L. Huerta Hernandez, J. Bertrandie, M. Babics, S. Alam, D. R. Villalva, S. H. K. Paleti, J. Gorenflot, C. Herok, N. Ramos, J. Troughton, A. Sharma, T. B. Marder, B. Engels, J. Martin, S. De Wolf, F. Laquai, D. Baran, *Joule* **2023**, *7*, 2135.
[150] S. Li, L. Zhan, F. Liu, J. Ren, M. Shi, C. Z. Li, T. P. Russell, H. Chen, *Adv. Mater.* **2018**, *30*, 1705208.
[151] H. Yu, Y. Wang, H. K. Kim, X. Wu, Y. Li, Z. Yao, M. Pan, X. Zou, J. Zhang, S. Chen, *Adv. Mater.* **2022**, *34*, 2200361.
[152] R. Ma, Q. Fan, T. A. Dela Pena, B. Wu, H. Liu, Q. Wu, Q. Wei, J. Wu, X. Lu, M. Li, W. Ma, G. Li, *Adv. Mater.* **2023**, *35*, 2212275.
[153] Y. Zhang, W. Deng, C. E. Petoukhoff, X. Xia, Y. Lang, H. Xia, H. Tang, H. T. Chandran, S. Mahadevan, K. Liu, P. W. K. Fong, Y. Luo, J. Wu, S.-W. Tsang, F. Laquai, H. Wu, X. Lu, Y. Yang, G. Li, *Joule* **2024**, *8*, 509.
[154] R. Sun, W. Wang, H. Yu, Z. Chen, X. Xia, H. Shen, J. Guo, M. Shi, Y. Zheng, Y. Wu, W. Yang, T. Wang, Q. Wu, Y. Yang, X. Lu, J. Xia, C. J. Brabec, H. Yan, Y. Li, J. Min, *Joule* **2021**, *5*, 1548.
[155] K. An, W. Zhong, F. Peng, W. Deng, Y. Shang, H. Quan, H. Qiu, C. Wang, F. Liu, H. Wu, N. Li, F. Huang, L. Ying, *Nat. Commun.* **2023**, *14*, 2688.
[156] Y. Li, X. Huang, H. K. M. Sheriff, S. R. Forrest, *Nat. Rev. Mater.* **2023**, *8*, 186.
[157] C. J. Traverse, R. Pandey, M. C. Barr, R. R. Lunt, *Nat. Energy* **2017**, *2*, 849.
[158] C. Ballif, L.-E. Perret-Aebi, S. Lufkin, E. Rey, *Nat. Energy* **2018**, *3*, 438.
[159] H. Yu, J. Wang, Q. Zhou, J. Qin, Y. Wang, X. Lu, P. Cheng, *Chem. Soc. Rev.* **2023**, *52*, 4132.
[160] C. Yang, D. Liu, M. Bates, M. C. Barr, R. R. Lunt, *Joule* **2019**, *3*, 1803.
[161] L. Duan, B. Hoex, A. Uddin, *Sol. RRL* **2021**, *5*, 2100041,.
[162] D. Wang, H. Liu, Y. Li, G. Zhou, L. Zhan, H. Zhu, X. Lu, H. Chen, C.-Z. Li, *Joule* **2021**, *5*, 945.
[163] W. Liu, S. Sun, S. Xu, H. Zhang, Y. Zheng, Z. Wei, X. Zhu, *Adv. Mater.* **2022**, *34*, 2200337.
[164] Y. Li, X. Guo, Z. Peng, B. Qu, H. Yan, H. Ade, M. Zhang, S. R. Forrest, *Proc. Natl. Acad. Sci. USA* **2020**, *117*, 21147.
[165] X. Liu, Z. Zhong, R. Zhu, J. Yu, G. Li, *Joule* **2022**, *6*, 1918.
[166] T. Xu, B. Deng, K. Zheng, H. Li, Z. Wang, Y. Zhong, C. Zhang, G. Lévêque, B. Grandidier, R. Bachelot, M. Treguer-Delapierre, Y. Qi, S. Wang, *Adv. Mater.* **2024**, *36*, 2311305.
[167] S. Guan, Y. Li, K. Yan, W. Fu, L. Zuo, H. Chen, *Adv. Mater.* **2022**, *34*, 2205844.
[168] S. Guan, Y. Li, C. Xu, N. Yin, C. Xu, C. Wang, M. Wang, Y. Xu, Q. Chen, D. Wang, L. Zuo, H. Chen, *Adv. Mater.* **2024**, *36*, 2400342.
[169] J. Ding, H. Mou, H. Chen, J. Xu, W. Sun, J. Zhu, Y. Wang, Y. Huang, Y. Li, Y. Li, *Adv. Mater.* **2025**, *37*, 2420439.
[170] X. Yuan, R. Sun, Y. Wu, T. Wang, Y. Wang, W. Wang, Y. Yu, J. Guo, Q. Wu, J. Min, *Adv. Funct. Mater.* **2022**, *32*, 2200107.
[171] D. Wang, R. Qin, G. Zhou, X. Li, R. Xia, Y. Li, L. Zhan, H. Zhu, X. Lu, H.-L. Yip, H. Chen, C.-Z. Li, *Adv. Mater.* **2020**, *32*, 2001621.
[172] G. P. Kini, S. J. Jeon, D. K. Moon, *Adv. Funct. Mater.* **2021**, *31*, 2007931.
[173] J. Yu, X. Liu, J. Zhou, G. Li, *Adv. Funct. Mater.* **2024**, *34*, 2406070.
[174] T. Ellenbogen, K. Seo, K. B. Crozier, *Nano Lett.* **2012**, *12*, 1026.
[175] M. Gaceur, S. B. Dkhil, D. Duché, F. Bencheikh, J.-J. Simon, L. Escoubas, M. Mansour, A. Guerrero, G. Garcia-Belmonte, X. Liu, M. Fahlman, W. Dachraoui, A. K. Diallo, C. Videlot-Ackermann, O. Margeat, J. Ackermann, *Adv. Funct. Mater.* **2016**, *26*, 243.
[176] W. J. Dong, N.-T. Lo, G. H. Jung, J. Ham, J.-L. Lee, *Appl. Phys. Lett.* **2016**, *108*, 103902.
[177] S. Wang, J. Chen, L. Li, L. Zuo, T.-Y. Qu, H. Ren, Y. Li, A. K. Y. Jen, J.-X. Tang, *ACS Nano* **2020**, *14*, 5998.
[178] X. Li, R. Xia, K. Yan, J. Ren, H.-L. Yip, C.-Z. Li, H. Chen, *ACS Energy Lett.* **2020**, *5*, 3115.
[179] Y.-H. Chen, C.-W. Chen, Z.-Y. Huang, W.-C. Lin, L.-Y. Lin, F. Lin, K.-T. Wong, H.-W. Lin, *Adv. Mater.* **2014**, *26*, 1129.
[180] X. Liu, Z. Zhong, Y. Li, Z. a. Li, J. Zhou, R. Zhu, J. Yu, G. Li, *Adv. Energy Mater.* **2023**, *13*, 2301361.
[181] C. Sun, R. Xia, H. Shi, H. Yao, X. Liu, J. Hou, F. Huang, H.-L. Yip, Y. Cao, *Joule* **2018**, *2*, 1816.
[182] N. Zhang, Z. Zhou, Y. An, F. Qi, R. Xia, G. Du, T. Xia, L. Ke, N. Li, F. R. Lin, A. K.-Y. Jen, H.-L. Yip, *Adv. Energy Mater.* **2024**, *n/a*, 2404129.
[183] D. Wang, Y. Li, G. Zhou, E. Gu, R. Xia, B. Yan, J. Yao, H. Zhu, X. Lu, H.-L. Yip, H. Chen, C.-Z. Li, *Energy Environ. Sci.* **2022**, *15*, 2629.
[184] Y. Zhao, Z. Li, C. Deger, M. Wang, M. Peric, Y. Yin, D. Meng, W. Yang, X. Wang, Q. Xing, B. Chang, E. G. Scott, Y. Zhou, E. Zhang, R. Zheng, J. Bian, Y. Shi, I. Yavuz, K.-H. Wei, K. N. Houk, Y. Yang, *Nat. Sustain.* **2023**, *6*, 539.
[185] G. Li, C. W. Chu, V. Shrotriya, J. Huang, Y. Yang, *Appl. Phys. Lett.* **2006**, *88*, 253503.

[186] J. Huang, J. Fu, B. Yuan, H. Xia, T. Chen, Y. Lang, H. Liu, Z. Ren, Q. Liang, K. Liu, Z. Guan, G. Zou, H. T. Chandran, T. W. B. Lo, X. Lu, C. S. Lee, H. L. Yip, Y. K. Peng, G. Li, *Nat. Commun.* **2024**, *15*, 10565.

[187] B. Liu, O. J. Sandberg, J. Qin, Y. Liu, S. Wilken, N. Wu, X. Yu, J. Fang, Z. Li, R. Huang, W. Zha, Q. Luo, H. Tan, R. Österbacka, C.-Q. Ma, *Nat. Photonics* **2025**, *19*, 195.

Ying Zhang received the Ph.D. degree in electronic and information engineering from The Hong Kong Polytechnic University under the supervision of Prof. Gang Li. She is currently a Postdoctoral Researcher at the University of California, Los Angeles, in Professor Yang Yang's group. Her research focuses on device engineering for high-efficiency and stable next-generation solar cells, with an emphasis on understanding the underlying device physics and operational mechanisms.

Yang Yang has completed the Ph.D. degree from the University of Massachusetts and postdoctoral studies from the University of California-Riverside. His major research interests are in solar energy and highly efficient electronic devices. He is currently the Carol and Lawrence E. Tannas Jr. Endowed Chair Professor and also serves as Chair of the Department of Materials Science and Engineering at UCLA. He is a fellow of the European Academy of Science, the American Association for the Advancement of Science, Materials Research Society, Royal Society of Chemistry, American Physical Society, Electromagnetic Academy, and SPIE, International Society for Optics and Photonics. Recently, he has received the following honors/awards: invited to join the Advanced Materials Hall of Fame (2021); Highly Cited Researcher in three major fields: materials science, chemistry, and physics, Thomson Reuters (now Clarivate Analytics) (2017, 2018, 2019); 2019 Sustainable Energy Award by UK Royal Society of Chemistry; Highly Cited Researcher in both Materials Science and Chemistry Categories (2013-2016, 2020&2022).

Gang Li is the Chair Professor of Energy Conversion Technology, Sir Sze-Yuen Chung Endowed Professor in Renewable Energy in the Department of Electrical and Electronic Engineering (EEE), the Hong Kong Polytechnic University. He serves as Director (HK) of Guangdong-Hong Kong-Macao Joint Laboratory for Photonic-Thermal-Electrical Energy Materials and Devices, and Associate Director of HK PolyU's Research Institute for Smart Energy (RISE). His research interests are the materials, device engineering and device physics in organic semiconductors and hybrid perovskite semiconductors, focusing on energy applications—solar cells, LEDs and photodetectors. He has published ≈300 papers, with ≈86 000 citations and H-index of 99 (Google Scholar). He has been a Highly Cited Researcher from 2014 to 2024 by Thomson Reuter/Clarivate Analytic. He is Fellow of Royal Society of Chemistry (UK), Optica (OSA), The International Society for Optics and Photonics (SPIE), Electromagnetic Academy, and Hong Kong RGC Senior Research Fellow.